CABLE STABILITY

L. Bottura
CERN, Geneva, Switzerland

Abstract
Superconductor stability is at the core of the design of any successful cable and magnet application. This chapter reviews the initial understanding of stability mechanism, and reviews matter of importance for stability such as the nature and magnitude of the perturbation spectrum and the cooling mechanisms. Various stability strategies are studied, providing criteria which depend on the desired design and operating conditions.

1 INTRODUCTION

The first superconducting magnets built in the decade around 1960 out of the newly available superconducting materials (mainly NbZr, Nb_3Sn and NbTi, in form of tapes or large monofilamentary strands) had their first transition to the normal state, i.e. a *quench*, much before reaching the expected critical current, disappointing largely the constructors. This happened in spite of the success in the development of the pure superconducting materials. The situation has been illustrated by Chester [1] in an excellent review article on the status of superconducting magnets development:

'[...] the development of superconducting solenoids and magnets has been far from straightforward, mainly because the behaviour of the materials in coils frequently did not accord with the behaviour of short samples. [...] The large number of coils [...] wound from Nb-Zr and Nb-Ti wire, and [...] Nb3Sn, revealed several intriguing and very frustrating characteristics of these materials in magnets.'

An example of this behaviour is shown in Fig. 1, reporting the history of the maximum current reached in a superconducting solenoid wound with a Nb-Zr wire. The magnet reached at the first powering only approximately 12 A, after which it quenched. At the following attempt to power the magnet, the current that could be reached before quench was higher. This process continued at each attempt, and the maximum current that could be reached increased quench after quench, slowly approaching a plateau, in the example of Fig. 1 at around 28 A. This behaviour became known as *training* [2], and the curve reported in Fig. 1 is called the *training curve*. The plateau current reached, however, was still below the expected maximum current carrying limit of the cable. As shown in Fig. 2 coils wound from a 0.25 mm Nb-Zr wire could achieve only a small fraction of the critical current of the single wire.

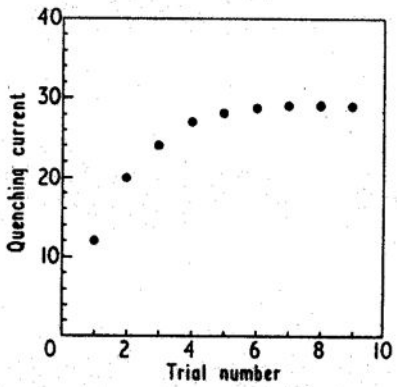

Figure 1. Training curve for an early Nb-Zr superconducting solenoid, reproduced from [1].

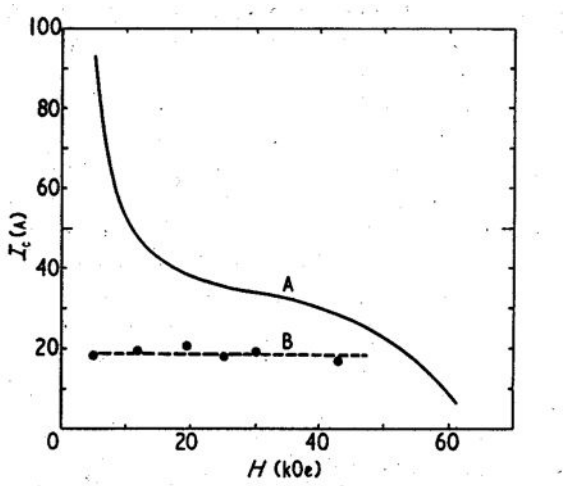

Figure 2. Typical critical current of a Nb-Zr superconducting wire (curve A) compared with that in coils producing the same field (curve B), reproduced from [1] (10 kOe = 1 T).

The current limitation observed was originally thought as originated by *bad spots* in the wires or cables, and thus attributed to bad homogeneity in the quality of the superconductor. This idea produced the concept of *degradation* of the conductor performance. Although training clearly showed that a physical degradation could not be responsible for the bad performance, the misleading name remained as an inheritance of the misty understanding. Particularly puzzling was the fact that the degradation depended on the coil construction and on its geometry. Quoting again Chester [1]:

'The prediction of the degraded current for any new shape or size of coil proved to be impossible and, for a time, the development of coils passed through a very speculative and empirical phase.'

A principle not yet fully understood at the time was that of *stability* of the cable with respect to external disturbances. Insufficient stability and large external disturbances were the key issue to the failure of the early experiments on superconducting magnets. It is since understood that a superconducting magnet is always subject to a series of energy inputs of very different nature, time scale and magnitude, the so called *disturbance spectrum* [3]. The energy input in the superconducting cable increases its temperature and can be sufficient to bring the superconducting material above critical conditions, where it becomes resistive and Joule heating is generated. The region that has transited to the normal resistive state is the so called *normal zone* in the magnet. Most materials at cryogenic temperature have a small heat capacity (ideally vanishing at the absolute zero), and the temperature margin, the difference between the operating temperature T_{op} and the temperature at which current sharing starts T_{cs}, must be kept small to achieve an economic design. The result is that the energy necessary to produce a normal zone can be small, typically in the range of tens to hundreds of μJ for few mm^3 of strand.

If not prevented by other mechanisms, the temperature in the normal zone increases further and the normal front propagates, so that the superconductor cascades from its nominal operating point into an irreversible process leading to the complete loss of superconductivity in the magnet, i.e. the magnet experiences a quench. This sequence of events is schematically shown in Fig. 3.

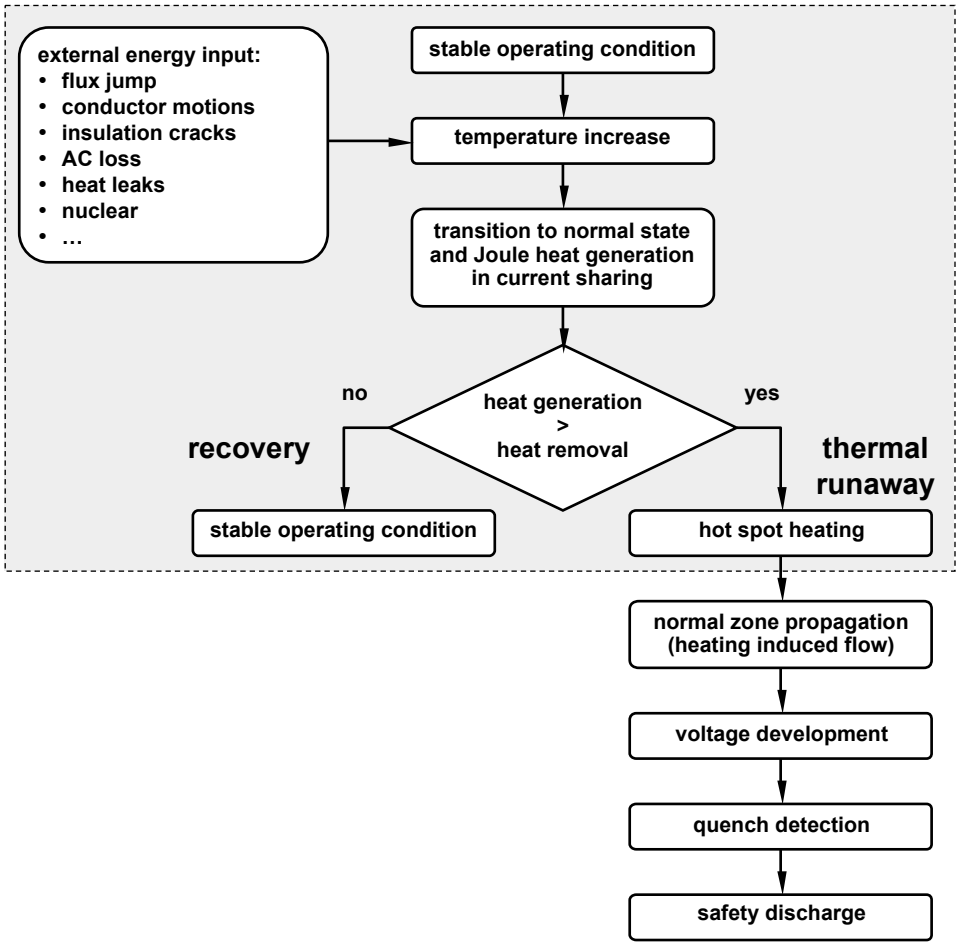

Figure 3. Event tree following an external energy input and leading from stable operating conditions back to stable operation or to a magnet quench. Stability design and analysis concentrate on the shaded area in the event tree.

Even if properly protected against damage a magnet quench is an undesirable event in terms of availability and cost. A well designed magnet will not quench under normal operating conditions. The study of stability has evolved through many years of experimentation and analysis towards the understanding of the processes and mechanisms whereby a superconductor remains (or not) within its operating region, thus ensuring *stable* operation of the magnet, i.e. free from quenches. With reference to the schematic representation of Fig. 3, stability is therefore mainly concerned with the phases in the event tree enclosed in the shaded area.

In spite of the substantial progress in understanding and improvement in the manufacturing techniques, stability is still one of the limiting factor for high performance magnets. As an example Fig. 4 reports the sequence of training quenches for an accelerator magnet, showing that to achieve high performance traning may still be necessary, while yet the expected short sample limit is not achieved. The training behaviour can be significantly different depending on manufacturing details such as the quality of the fitting of the mechanical structure and the coil windings.

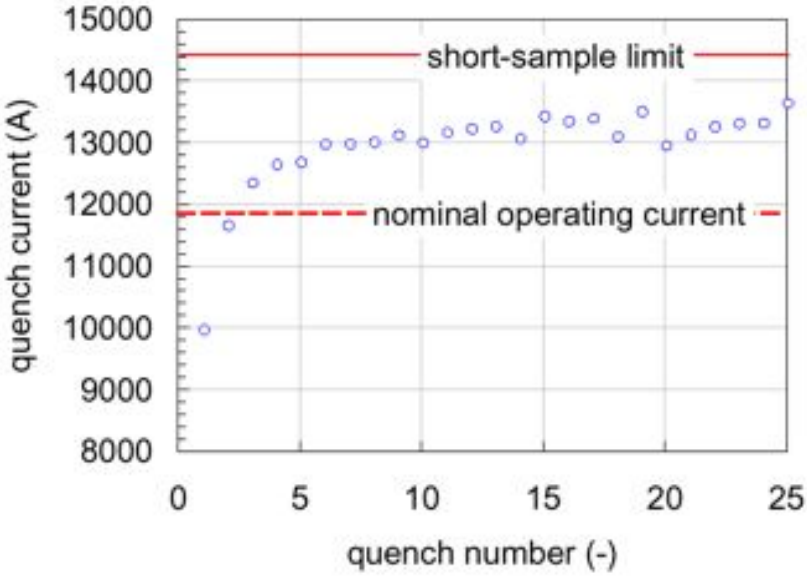

Figure 4. Sequence of training quenches for a short model of an LHC dipole magnet, showing the initial, short training period necessary to reach nominal operating conditions and a plateau current reached after several quenches still below the expected short sample limit.

This chapter deals with cable stability under most common conditions found in superconducting magnet design. The first step in a sound design is to estimate the envelope of the perturbations that will be experienced by the magnet. Typical energy and time scales of the perturbation spectrum are reviewed in Section 3.2. The conductor can then be designed to accommodate these perturbations by means of a sufficiently large stability margin, using the concepts discussed in Sections 3.6 (adiabatic stabilization), Section 3.7 (cryostability), Section 3.8 (cold-end recovery and equal area theorem), Section 3.9 (well-cooled operation for force-flow cooled conductors) and Section 3.10 (minimum propagating zone). Appropriate examples based on existing magnets are given in each section. In order to develop the relevant concepts and techniques we will introduce in Section 3.3 a general form of the heat balance for a superconducting cable and in Sections 3.5 and 3.6 we will discuss the details of heat generation during current sharing and steady state and transient heat transfer to a cryogenic coolant. Finally, in Section 3.11 we discuss some advanced topics (current distribution) in stability design and analysis.

2 PERTURBATION SPECTRUM

Several mechanisms can cause the generation of heat in a superconducting cable carrying a current in a magnetic field and operating in a cryogenic environment. These perturbations are distributed over a wide spectrum with large differences in magnitude and time scale depending on the origin of the perturbation itself. Some disturbances can be extremely localised in space and time, e.g. mechanical energy release due to a small motion of a superconducting wire, and can initiate only normal zones of small volume. Other disturbances can affect large portions of a superconducting magnet and last a significant time, e.g. AC loss for pulsed operation or heat deposition from nuclear processes in a superconducting accelerator magnet, and thus they can potentially produce normal zones with large volume. The specific perturbation spectrum for a particular application depends on the design of the superconducting magnet and on the operating conditions of the system, and is difficult to generalise.

In this section we give a sample of most common disturbances, and their associated energy, volume and time scales. Stability analysis and design is mostly concerned with transient perturbations with limited duration in time. Hence they can be characterised by the total energy deposited during the transient in units of [J]. For the comparison of different phenomena acting on different volumes it is

useful to reason in term of energy density referred to the total cross section of the conductor. This quantity is usually quoted for practical resons in units of [mJ/cm^3] as then the typical values range from fractions of unit to few hundreds.

Continuous heat deposition, as is the case for heat leaks from room temperature, are rather characterised by the heating power, measured in units of [W] for localised inputs, in units of [W/m^2] for surface heat loads or units of [W/m^3] for volumetric loads. These perturbations, although very important for the overall performance of a system, are usually not the concern for stability. They are dealt with by proper sizing of the thermal insulation and cooling system. It is nonetheless interesting to show the corresponding energy deposited over the typical time scales of interest for stability, also discussed here in units of [mJ/cm^3] to provide comparable dimensions.

2.1 Flux jumps

A small heat input into a superconductor in a magnetic field, due for example to any of the reasons discussed below, causes a decrease of the critical current density J_c through the temperature increase (all technical superconductors have a negative $J_c(T)$ slope). In adiabatic conditions, the magnetisation of the superconductor (proportional to the current density) also decreases, resulting in a penetration of the external magnetic field in the superconducting bulk. A part of the energy stored in the magnetisation profile is therefore dissipated resistively within the superconductor. The energy release caused by the decrease of the magnetisation can be sufficient to cause an irreversible transition of the wire to the normal state - a *flux jump*.

In order to estimate the maximum possible energy release during a flux jump we can make the assumption that during the transient the magnetization of a superconducting filament disappears because of the process described above. To simplify matters in this study, we approximate the filament as a plane slab with thickness D identical to the diameter of the filament. Following a ramp of increasing magnetic field up to a value B much larger than the penetration field, and neglecting the influence of transport current, the shielding currents fill the slab, in fully penetrated state.

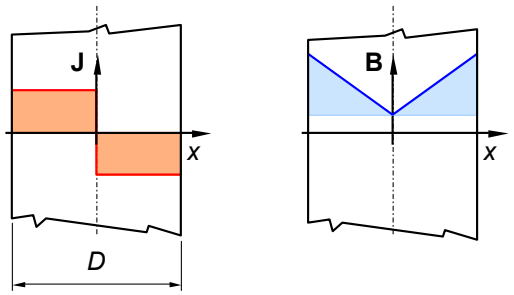

Figure 5. Profile of magnetic field and current density in a fully penetrated superconducting filament, ideally represented by a slab of thickness D along x and infinite extension in the two other dimensions. The area shaded in the plot of the field profile disappears during a complete flux jump.

The magnetic field contribution δB due to the shielding currents has a dependence on the position x given by:

$$\delta B = \mu_0 J_c x \tag{1}$$

where J_c is the critical current density of the superconductor. The field profile is shown in Fig. 5. Following a complete flux jump the energy stored in this field profile is dissipated resistively inside

the filament. The average energy dissipation Q''' per unit volume of the filament can then be calculated as follows:

$$Q''' = \frac{2}{D}\int_0^{D/2} \frac{\delta B^2}{2\mu_0} dx = \frac{\mu_0 J_c^2 D^2}{24} \quad (2).$$

From the above expression we can estimate the energy density released during a flux jump in a typical superconductor such as Nb-Ti. Assuming that J_c is 5000 A/mm^2 and a filament diameter D of 50 μm we obtain an energy density of 3 mJ/cm^3. This energy can be released extremely fast, typically in tens of μs up to fractions of ms, and is sufficient to increase adiabatically the temperature of a Nb-Ti strand by few degrees.

The magnetisation of a fully penetrated superconducting filament is proportional to the size of the filament, and the energy stored in the trapped magnetic field is proportional to the square of the filament size as shown by Eq. (2). Because of this flux jumps were a principle problem at times when superconducting material technology did not allow to produce a fine subdivision of the superconductor in the wire. In fact, flux jumps were among the first perturbations recognised to be responsible for performance degradation, and thus intensely studied in the late 60's and early 70's (see for instance the review of Rutherford Laboratory Superconducting Applications Group [4]), leading to one of the first quantification's of the idea of a disturbance spectrum. Because of this, the early considerations of stability were often interleaved with flux jumps theory.

Fine subdivision in small filaments is the most obvious cure of flux jumping. On one side it reduces the energy dissipated as clear from Eq. (2) and therefore it eases the so called *adiabatic* stabilisation. On the other hand, fine subdivision means an increase of the superconductor surface, making it easier to remove efficiently the heat generated by the flux penetration in the bulk superconductor, the so called *dynamic* stabilisation. Nowadays flux jumps are no longer a problem for standard production of low-temperature superconducting wires (typically based on NbTi and Nb_3Sn materials). Flux jumps may still play some role in high-temperature superconductors operated at low temperatures (around and below 20 K), although the steadily improving technology is quickly making this statement obsolete.

2.2 Mechanical events

A superconducting magnet is always subjected to stresses, either from pre-loading at assembly, differential thermal contractions at cool-down or resulting from the electromagnetic forces at operation. The forces acting on a superconducting cable can induce small movements. In some cases the stress can be large compared to the elastic and failure limits of the materials, and displacement can take place as a result of material yeld or fracture. Any displacement causes a change in the stress state associated with a release of a part of the mechanical energy stored. The release of the mechanical energy can happen locally through micro-slips constrained by friction, material yelding, vibration, local cracking [5].

We can appreciate the amount of mechanical energy associated with one of the above events by estimating the energy release due to an hypothetical strand motion. A strand operating at a current I_{op} in a transverse field B_{op} results in a Lorentz force F' per unit length of the strand of:

$$F' = I_{op} B_{op} \quad (3).$$

Taking typical values for the bending magnets of a particle accelerator, I_{op} of 400 A and B_{op} of 10 T, the force per unit length is F' = 4 kN/m. This force is reacted against the other wires in the winding

pack and the structure of the magnet. However, even in a tightly packed winding the wire can move by small distances, because of the geometrical tolerances on the wire dimension and the limitations on the control of the winding geometry. Movements δ of few μm over strand length l of few mm are not uncommon if the winding pack is not fully impregnated. The work W performed by the Lorentz force during a movement δ can be calculated as:

$$W = F'\delta\, l \tag{4}.$$

A movement of 10 μm of a length of 1 mm of a single strand under the conditions given above is associated with a work W = 40 μJ. This work corresponds to an energy density of:

$$W''' = \frac{F'\delta}{A_{strand}} \tag{5}.$$

where A_{strand} is the total strand cross section. For a strand with 1 mm^2 cross section, typical of the application considered, the energy density is 40 mJ/cm^3. The mechanical work is partially dissipated as friction against the other wires and partially as a resistive loss induced by the electric field on the moving wire. The percentage of energy dissipation depends on the detail of the process and cannot be estimated easily, ranging from only few percent to large fractions of the above estimate. These events take place on few mm^3 of cable, and are fast, with typical times that are generally ranging from tens of μs to few ms.

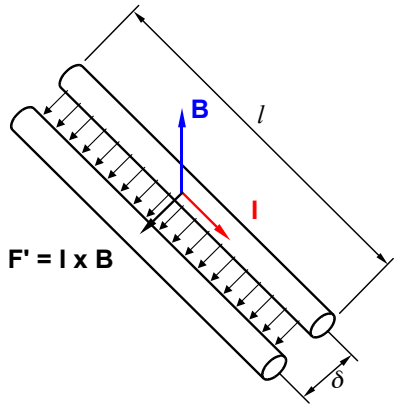

Figure 6. Schematic representation of a strand motion in a magnetic field. The strand length l is subjected to a transverse electromagnetic load F' per unit length and moves by a length δ in the direction of the force.

In few cases thermal or magnetic stresses become large enough to cause some part of the structural materials to yeld, or to fracture depending on the embrittlement at low temperature. Under these circumstances more massive disturbances are produced such as de-bonding or shear failure of the insulation or displacement of a part of the magnet. Heat is released in these processes through friction during motion, or once the movement is stopped. These *massive* processes are however rarely taking place at the single cable level, but rather at the mechanical interface between coil winding and supporting structures. Hence they are generally produced at some distance from the superconducting wire, and energy reaches the superconductor only after a diffusion process through structural components and/or the insulation. For this reason although the energy release is large, reaching potentially thousands of mJ/cm^3, and affects large coil volumes, the time scale for the energy release is long and thus the associated power is small. In spite of this, particular care must be applied when designing critical areas in a coil system such as the interface between coil winding and mechanical

structure (e.g. coil flanges and formers for solenoids), interfaces between winding parts (e.g. mating surfaces of segmented magnets), coil interconnections (e.g. soldered joints between windings) aiming on one side at avoiding displacements and on the other hand at minimising the energy release following the unavoidable deformations.

2.3 Electromagnetic transients

In several cases superconductors must be either designed for pulsed operation (e.g. transformers, power cables, SMES systems) or must be able to withstand transient changes of the self and background magnetic field (e.g. effect of a plasma disruption in a superconducting magnet system of a thermonuclear experiment, trip of normal resistive inserts in a hybrid solenoid). In any case all superconducting magnets, whether designed for steady state or pulsed operation, must be ramped to the operating condition. Hence operation of a superconductor in a magnet is always associated to more or less severe conditions on the variation of the field seen by the cable.

Any field change, on the other hand, produces energy dissipation through hysteresis or coupling AC loss in superconducting filaments, strands or cables. The time scale of the energy deposition in this case is governed by the dynamic of the magnetic field as well as the time constant of the induced persistent or coupling currents, and can cover a large span of characteristic time from few ms up to quasi steady state heating conditions for AC operation. The energy deposited by AC loss can also vary largely depending on the field change, its time scale and the characteristics of the superconductor.

In well designed cables the AC loss deposited during pulsed operation or fast field transients (typical field variations of few T/s lasting 10 to 100 ms) ranges from few mJ/cm^3 to few hundreds of mJ/cm^3. Larger energy deposition is usually avoided by small filament diameter, thus reducing hysteresis loss, and placing resistive barriers in the strands and within the cable, thus reducing coupling loss. Continuous operation with AC excitation results in distributed power deposition ranging from 0.1 W/m^3 of cable to 100 W/m^3 for the most demanding conditions. The typical time necessary to reach regime conditions for continuous operation is 0.1 to 1 s.

2.4 Heat leaks

All superconducting magnets operate at temperatures in the cryogenic range. A common source of heat is therefore represented by leaks entering through the thermal insulation of the magnet, the supporting structure, current leads and instrumentation wires. Although minimized by proper design, heat inleaks cannot be completely avoided and are removed by direct or indirect cooling. Heat through the insulation and supports in normal conditions, as well as loss of cooling or degraded cooling in abnormal operating conditions, generally result in broadly distributed heat sources of potentially large deposited energy but low power and nearly steady state characteristic. Heat leaks from instrumentation wires or current leads can lead to more localised energy inputs, with however long time scales of energy deposition.

The typical heat loads due to common heat leaks have a broad range of values depending on the size and operating conditions of the magnet system. Expected values for an accelerator magnet are few W, while for the magnetic system of a fusion reactor the heat load represented by current leads and heat leaks can amount to few kW. The corresponding power density referred to the cable volume in the magnet ranges from 0.1 to 10 W/m^3. Higher power density can be reached for localised inputs such as a high resistance superconducting joint or a badly thermalised instrumentation wire. The characteristic time for the establishment of regime conditions for the heat load associated with current leads or heat leaks and degraded cooling is from several s up to several hundreds of s.

2.5 Other sources

One additional source of energy in superconducting magnet systems used either in nuclear physics experiment or thermonuclear reactors is the heat deposited by nuclear interactions during normal and abnormal conditions. One of the most severe examples is the nuclear shower following a partial or complete loss of beam in the steering magnets of a particle accelerator, leading to energy deposition of few mJ/cm^3 to few tens of mJ/cm^3 in short times, in the ms range, and localised over a length of few m, small compared to the overall accelerator size but still affecting large volume portions of a magnet.

Superconducting magnet systems for thermonuclear reactors sustain a neutron flux generated by the fusion reaction. As for the continuous heat loads discussed in the previous section, although the nuclear heat can be large, the heat is deposited over long pulses, several s, and has thus nearly steady state characteristics. The corresponding power density ranges from 10 to 100 W/m^3.

2.6 Summary of perturbation spectrum

Figure 5 shows a summary of the energy that can be deposited by the various mechanisms discussed above in a superconducting magnet as a function of the characteristic time for the energy deposition, the *perturbation spectrum*. The values reported are intended to represent a guideline for the typical orders of magnitude, and do not necessarily apply to a specific magnet system, nor do they all appear simultaneously in a given magnet systems, and should be therefore used with caution. The representation of Fig. 7 shows however clearly that on the time scale of fast energy deposition (below 1 ms) the dominating mechanisms are those associated with wire and conductor motion. Flux jumps with superconducting strands based present technology are masked by the more energetic mechanical events. At intermediate time scales, in the range of few ms to few hundreds of ms, the dominating energy perturbation in pulsed magnets is generated by AC loss. For magnets operated in steady state in nuclear environments, e.g. particle accelerators, AC loss is negligible and the main concern in this time scale are events associated with particle showers and nuclear heat. Finally, if the magnet system operats in steady state condition and in a *quiet* environment, e.g. MRI and laboratory magnets, the dominating events are those associated with conductor motion at the fast time scale. For longer times, above 1 s, the dominating perturbations are generated by the steady state heat loads (heat leaks, nuclear heat, AC loss) and are no longer a direct stability concern as on this time scale the heat is usually evacuated by the cooling system.

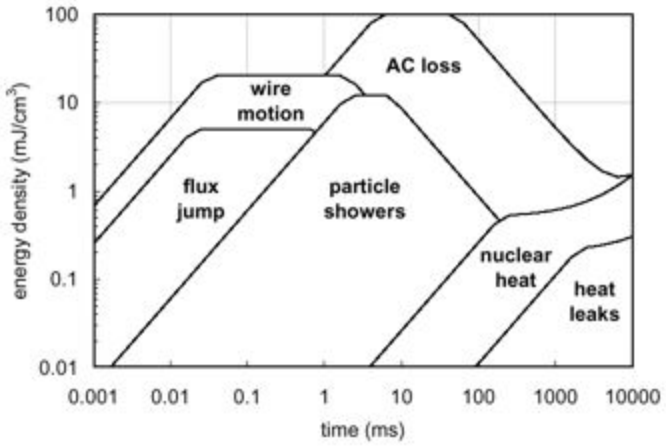

Figure 7. Typical spectrum of energy perturbations during normal operation of superconducting magnets. The energy deposited by different processes discussed here is plotted as a function of the characteristic time of energy deposition. Values are indicative and are intended to compare orders of magnitude.

3 HEAT BALANCE

The temperature of a superconducting cable changes following the energy input associated to one of the perturbations discussed in the previous section. The evolution of the temperature of the cable is governed by a transient heat balance containing in the most general case:

- the heat generation term representing the external perturbation
- the Joule heating term, appearing as soon as the superconductor exceeds the current carrying capability,
- the heat sink associated with the enthalpy of the cable,
- heat conduction along the cable and across the winding,
- and heat exchange with a coolant, with possibly limited heat capacity and stagnant or flowing along the cable.

This situation is schematically depicted in Fig. 8.

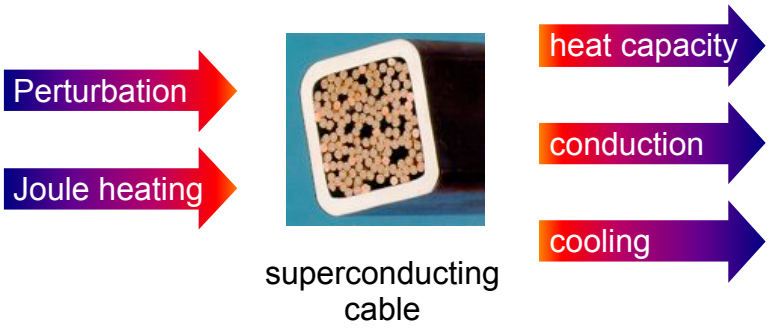

Figure 8. Terms contributing to the heat balance governing the evolution of the temperature of a superconductor following the energy input associated with one of the perturbations sources discussed.

The specific form of the heat balance depends on the details of the cable considered. Accordingly, the temperature evolution, and in last analysis the stability of the superconductor, is different for different cables. The governing equation is relatively simple in the case that the conductor can be approximated as an adiabatic strand, in which case the conduction and cooling terms disappear and analytic treatment is appropriate. On the other hand in the case of a cable as used for large scale applications cooled by a forced flow of helium, the terms of the equation can have a complex mathematical structure and the solution of the heat balance requires extensive numerical treatment

In order to the discuss the main concepts necessary for understanding the most inportant features of superconductor stability we focus on the ideal case of a superconducting cable operating at a current I_{op} in a background magnetic field B_{op} and an initial temperature T_{op}. The external energy input has a power density q'''_{ext} referred to the whole cable cross section A consisting of a superconductor portion A_{sc} and a stabilizer, a low resistive material whose function will be discussed later, of cross section A_{st}:

$$A = A_{sc} + A_{st} \tag{6}$$

Although other materials such as resistive barriers or structural materials could be included, we neglect them for the moment for the sake of simplicity. The cable temperature T evolves following the perturbation, but it is assumed to be uniform across the cable transverse dimension. In addition we

make the hypothesis of uniform current distribution among the strands of the cable. The cable is cooled by a helium bath at temperature T_{he}. Once again, for the sake of simplicity, the helium bath is considered as stagnant and with an infinite heat capacity so that T_{he} is constant. The heat exchange between cable and helium takes place over a *wetted perimeter w* and is characterised by a heat transfer coefficient *h*.

Under these conditions the temperature of the cable evolves in accordance with the following equation that is obtained from the balance of heat sources and heat sinks:

$$C\frac{\partial T}{\partial t} = q'''_{ext} + q'''_J + \frac{\partial}{\partial x}\left(k\frac{\partial T}{\partial x}\right) - \frac{wh}{A}\left(T - T_{he}\right) \tag{7}.$$

In the above balance *C* and *k* are the cable volumetric heat capacity and thermal conductivity defined as a weighted average of the properties of the superconductor and of the stabilizer (subscripts *sc* and *st* respectively):

$$C = \frac{A_{sc}\rho_{sc}c_{sc} + A_{st}\rho_{st}c_{st}}{A} \tag{8}$$

$$k = \frac{A_{sc}k_{sc} + A_{st}k_{st}}{A} \tag{9}$$

where c_{sc} and c_{st} are the specific heats, ρ_{sc} and ρ_{sc} are the mass densities, k_{sc} and k_{st} are the thermal conductivities. The term q'''_J stands for the heat per unit cable volume generated when the superconducting material is driven above critical conditions, in the so called *current sharing* regime. This is the topic of the following section, and for the moment we simply assume that q'''_J is zero when the superconductor is operating below critical conditions, and different from zero above.

A sample of a typical temperature evolutions following an energy perturbation in a superconducting cable as described by the heat balance Eq. (7) is shown in Fig. 9. The external perturbation inducing the thermal transient is assumed to deposit its energy over a time of 10 ms. Without entering in the details of the results reported there, we note that initially the temperature of the superconductor increases sharply as a consequence of the heat input provided by the perturbation. After the end of the energy pulse the temperature initially drops under the effect of the heat conduction and cooling heat fluxes. If the conduction and cooling are sufficient the cable recovers the superconducting state and eventually returns to stable operating conditions, i.e. the curve marked as *recovery* in the plot of Fig. 9. If the cooling is insufficient, after the drop the cable temperature starts again to rise under the predominating contribution of Joule heating, eventually leading to the quench shown by the curve indicated as *thermal runaway* in Fig. 9.

The balance among the non-linear Joule heating and the cooling terms is extremely delicate and can be displaced by small changes in the perturbation energy. Based on the qualitative features discussed above, it is possible to define an *energy margin* $\Delta Q'''$ as the minimum energy density that the external source needs to provide to the cable to cause a thermal runaway. An energy input larger than $\Delta Q'''$ causes a thermal runaway, while an energy input smaller than $\Delta Q'''$ leads to a recovery. For consistency with our discussion on the perturbation spectrum we measure the energy margin in units of [mJ/cm^3]. Often in the literature the energy margin is also quoted as *stability margin*, with the same definition above. For perturbations of known and limited distribution in space it can be useful to refer to the *minimum quench energy* ΔQ (MQE) that corresponds to the integral in space of the energy margin and is thus measured in units of [J].

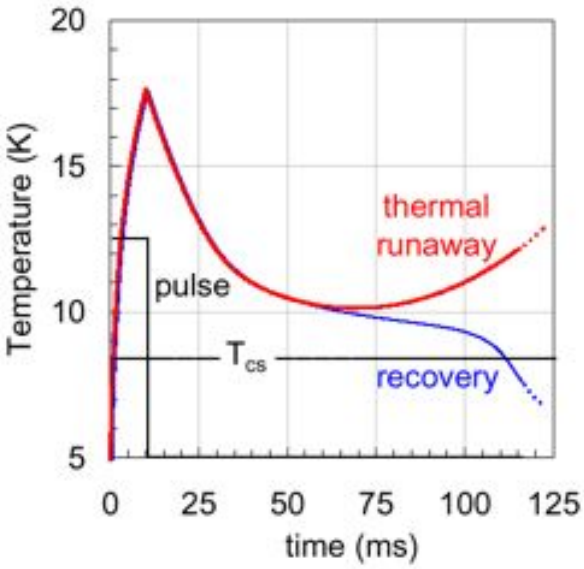

Figure 9. Qualitative evolution of the temperature in a superconducting cable for an energy perturbation just below and just above the energy margin. The former leads to a recovery, while the latter results in a thermal runaway.

4 CURRENT SHARING

An ideal superconductor becomes resistive if one of the three parameters, current density, temperature or magnetic field, exceeds the boundary of the critical surface $J_c(B,T)$, and in these conditions the current flow is associated with resistance and Joule heating in the cable. This is schematically shown in Fig. 10 showing the temperature dependence of the critical current I_c of a superconducting cable, defined as the product of critical current density and superconductor cross section:

$$I_c = J_c A_{sc} \tag{10}.$$

When the cable operates at a temperature T_{op} below the critical current the material is superconducting. This situation can be ideally maintained also at a temperature above T_{op} provided that the operating current is still smaller than the critical current. The temperature at which the critical current equals the operating current is called the *current sharing temperature* T_{cs}. Above T_{cs} the superconductor develop a resistance and current flow is associated with Joule heating. The difference between the current sharing temperature and the operating temperature is often referred to as the temperature margin ΔT.

Technical low- and high-Tc superconductors have a high resistivity in normal state compared to normal conductors in cryogenic conditions. As an example NbTi has a normal state resistivity η_{sc} of the order of 6.5 10^{-7} Ωm, while copper and aluminium have typical low temperature resistivity η_{st} of few 10^{-11} Ωm to 10^{-10} Ωm depending on the degree of purity and on the background magnetic field. As intuitive, and discussed later in detail, a decrease in heat generation is always beneficial for stability. For this reason, in addition to protection and manufacturing considerations, superconducting strands are nearly always built as a composite containing both superconducting material and a normal conducting *stabilizer* material with low resistivity in intimate mechanical, thermal and electrical contact.

The normal conducting stabilizer acts as a low resistance shunt in case of transition of the superconductor to the normal state, in what is called the *current sharing* process. A good

representation of current sharing can be achieved considering the superconductor and the stabilizer as parallel resistors, as shown schematically in Fig. 11. For the moment we ignore the details of the current distribution within the strand cross section, a safe hypothesis in the time scales of interest for stability for common strands but insufficient when dealing with super-stabilized conductors, as will be discussed in a later section.

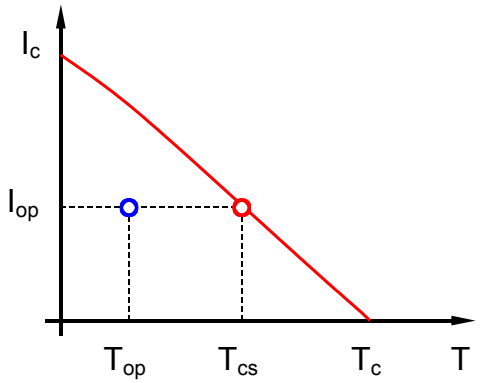

Figure 10. Critical current dependence on temperature and definition of the current sharing temperature.

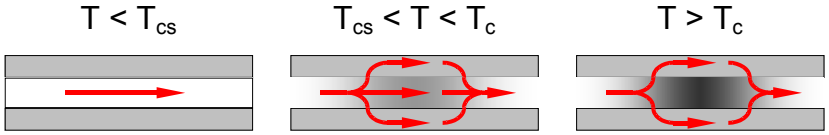

Figure 11. Current sharing in a composite strands consisting of a superconductor and a normal conducting material. The situation is shown for operation below the critical surface of the superconductor, in current sharing conditions, at a temperature between the current sharing temperature and critical temperature, and above the critical temperature.

For operating temperature below T_{cs} the whole operating current I_{op} flows in the superconductor with zero resistance and no Joule heating. For operating temperature between T_{cs} and T_c the superconductor develops a longitudinal resistive voltage. Under this voltage a part of the current is transferred from the superconductor to the stabilizer. The current in the stabilizer also produces a longitudinal resistive voltage, and in equilibrium conditions this is equal to the voltage in the superconductor. The amount of current transferred depends on the electrical characteristics of the superconductor (in normal state) and of the stabilizer. As discussed above, the normal state resistivity of the superconductor is much larger than that of the stabilizer. This corresponds to the voltage-current characteristic schematically shown in Fig. 12, with zero resistivity up to the critical current and infinite resistivity above.

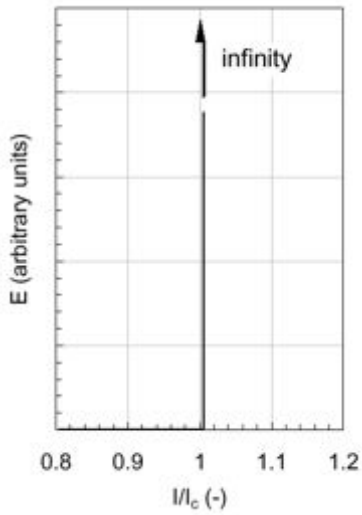

Figure 12. Voltage-current characteristic of an ideal superconductor. The resistivity is large in normal state, for a ratio of operating current to critical current above 1. In these conditions the longitudinal electric field has an ideally infinite value.

In this condition the current transferred to the stabilizer is exactly the current in excess of the critical current, or:

$$I_{st} = I_{op} - I_c \tag{11}$$

while the superconductor carries the current I_c. The longitudinal electric field E in the stabilizer (and in the superconductor) is given by:

$$E = I_{st} \frac{\eta_{st}}{A_{st}} \tag{12}$$

and the Joule heat power density in the cable can be calculated as follows:

$$q'''_J = \frac{EI_{st} + EI_{sc}}{A} = \frac{EI_{op}}{A} = \frac{\eta_{st}}{A_{st}} \frac{I_{op}\left(I_{op} - I_c\right)}{A} \tag{13}.$$

Finally, for an operating temperature above T_c, the critical current of the superconductor is zero and the whole current flows in the stabilizer. In this case the longitudinal electric field is:

$$E = I_{op} \frac{\eta_{st}}{A_{st}} \tag{14}$$

and the Joule heat power density is given by:

$$q'''_{J\max} = \frac{\eta_{st}}{A_{st}} \frac{I_{op}^2}{A} \tag{15}.$$

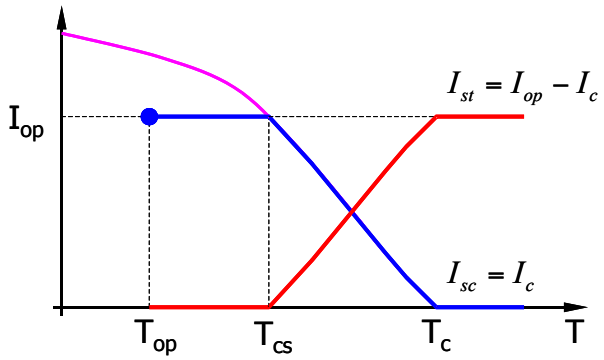

Figure 13. Current sharing among the superconductor and the stabilizer as a consequence of a temperature change.

The situation described above is shown schematically in Fig. 13. We see by direct comparison of Eqs. (13) and (15) that the maximum Joule heating is reached in the condition $T > T_c$ as expected. So far no we have made assumptions on the temperature dependence of the critical current, and the expressions derived above are quite general. It is however customary to take a line approximation for the $I_c(T)$ dependence, writing that:

$$I_c \approx I_{op} \frac{T_c - T}{T_c - T_{cs}} \tag{16}.$$

In this case we can write explicitly the temperature dependence of the longitudinal electric field in the current sharing regime:

$$E = I_{op} \frac{T - T_{cs}}{T_c - T_{cs}} \frac{\eta_{st}}{A_{st}} \tag{17}$$

which is also a linear function of temperature, rising from zero at the current sharing temperature T_{cs} to its maximum at the critical temperature T_c. The Joule heat power density is given by:

$$q'''_J = \begin{cases} 0 & \text{for} \quad T < T_{cs} \\ q'''_{J\max} \dfrac{T - T_{cs}}{T_c - T_{op}} & \text{for} \quad T_{cs} < T < T_c \\ q'''_{J\max} & \text{for} \quad T > T_c \end{cases} \tag{18}$$

where the maximum Joule heating power density is defined as in Eq. (15). The functional dependence reported in Eq. (18) is represented schematically in Fig. 14. Note the non-intuitive linear increase of the Joule heating power between T_{cs} and T_c.

The ideal situation discussed so far provides a fair description of most situations, with a simple *caveat* on the fact that the stabilizer resistivity entering the expressions above usually has a strong dependence on the magnetic field below 20 K and on temperature above 20 K. Once this dependence is taken into account the result of Eq. (15) and (18) can be used for most practical cases.

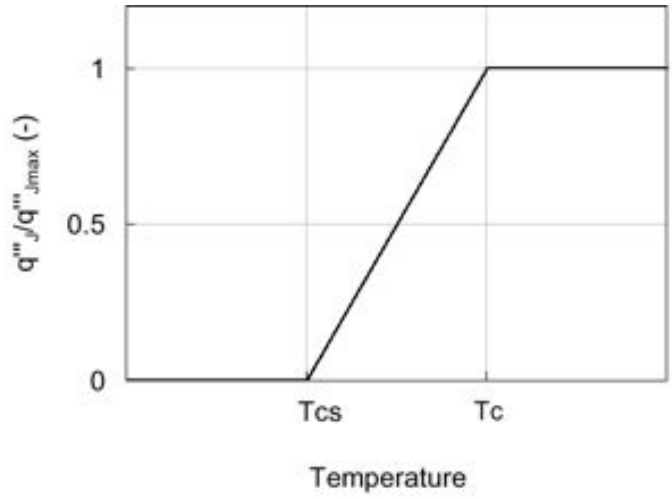

Figure 14. Joule heating power as a function of temperature, normalised to the maximum value reached for operation above T_c.

In particular situations, e.g. dealing with operating conditions at few percent from the critical current, or when considering large cables manufactured with several hundreds to thousand strands, it is necessary to correct the above result to achieve an accurate description. In these particular cases it is no longer sufficient to use the asymptotic voltage-current characteristic shown in Fig. 12. A better description for the resistive transition of the superconductor is achieved using for instance the power-law approximation given by:

$$E = E_0 \left(\frac{I_{sc}}{I_c} \right)^n \tag{19}$$

where E_0 is the electric field used as a criterion for the definition of the critical current and n is the exponent defining the *sharpness* of the transition. The power-law has the form shown in Fig. 15.

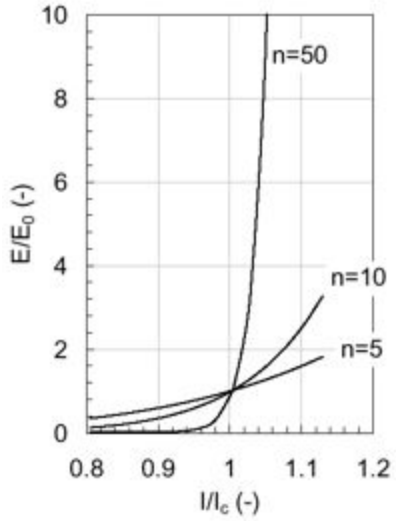

Figure 15. Normalised voltage-current characteristic of a superconductor characterised by a power-law dependence of the resistive voltage on the current, with exponent n. The voltage-current characteristic is plotted for different values of the exponent n.

A low value of the exponent *n* corresponds to a shallow and broad transition, while a high value of the exponent *n* gives a sudden transition. Note also that low exponent *n* corresponds to the appearance of a resistive voltage *before* reaching the critical current. We should therefore expect that a small portion of the operating current is transferred to the stabilizer already below critical conditions. Finally, the ideal limit used so far is achieved when the exponent *n* tends to infinity.

The current sharing between the superconductor described by the power-law and the stabilizer can be computed equating the longitudinal electric field as done previously. The electric field in the superconductor is given by Eq. (19). For the stabilizer Eq. (12) still holds, which we however rewrite as follows:

$$E = \left(I_{op} - I_{sc}\right)\frac{\eta_{st}}{A_{st}} \tag{20}.$$

The equilibrium condition is that:

$$E_0\left(\frac{I_{sc}}{I_c}\right)^n = \left(I_{op} - I_{sc}\right)\frac{\eta_{st}}{A_{st}} \tag{21}$$

that cannot be solved analytically for an arbitrary value of the exponent *n*. It is however possible to solve Eq. (21) numerically, obtaining the value of the current in the superconductor and in the stabilizer. The Joule heat power density is then computed as in Eq. (13), where this time the simplest form is obtained as:

$$q'''_J = \frac{EI_{st} + EI_{sc}}{A} = \frac{EI_{op}}{A} \tag{22}.$$

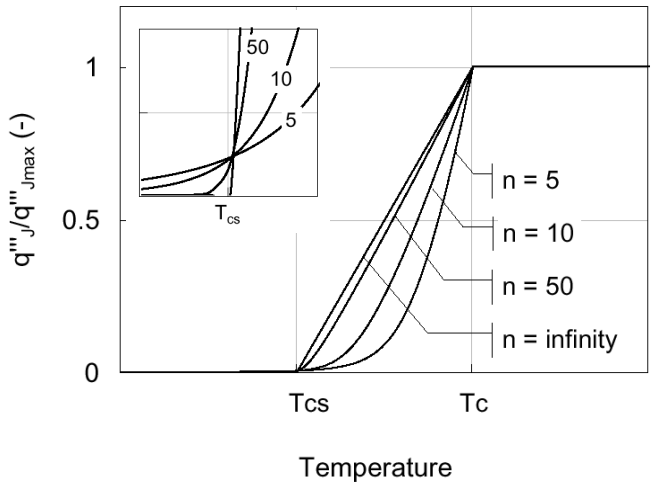

Figure 16. Normalised Joule heat dependence on temperature for a superconductor with a power-law voltage-current relation. The normalised heat generation is plotted for for different values of the exponent *n* and compared to the ideal case obtained for an infinite value of *n*. The inset shows a detail of the heat generation in the vicinity of the current sharing temperature T_{cs}.

A sample of numerical solution obtained for the normalised heat generation is shown in Fig. 16. We note that low values of the power-law exponent n correspond to smaller heat generation in the current sharing regime, between T_{cs} and T_c. The implications for stability of this fact will be discussed later. On the other hand, a peculiar feature to be remarked in the case of low n is that the Joule heating starts already before reaching T_{cs}, consistently with the appearance of an electric field already below critical conditions as discussed earlier. In fact, early current sharing and Joule heating at low n can be a limiting factor for operation at a high fraction of the critical current, and for this reason a high value of the exponent n is considered an indicator of the good quality of the strand or cable. Finally see how the linear limit given by Eq. (18) is approached when n is large, as expected.

5 HEAT TRANSFER

With the only exception of superfluid Helium, heat transfer in cryogenic fluids has been found to be very similar to the one predicted by standard thermodynamics. Proper allowance must be made for the fact that the thermophysical properties at the operating point of relevance are very different from those of room and high temperature coolants. Apart from this, however, the correlations available in literature for the various room and high temperature heat transfer regimes are essentially valid also in cryogenic conditions with small adaptions. For low-temperature superconducting magnets two regimes are of particular relevance, namely boiling heat transfer to a stagnant bath of atmospheric pressure, saturated liquid helium (temperature around 4.2 K, approximately 1 bar) and forced-flow convection of supercritical helium (temperature in the range of 4.5 K, pressure above 3 bar). For these two regimes we will give practical correlations and typical values of heat transfer that will be used later in the discussion. In addition in more recent years, following the advancement in the technology necessary to produce superfluid helium, cooling in a bath of stagnant, subcooled superfluid helium at atmospheric pressure is used in several small and large size applications. Heat transfer in superfluid helium is peculiar and we will therefore discuss a simple approximation to this process.

5.1 Boiling heat transfer

Cooling of the the first large size superconducting magnets, such as the Big European Bubble Chamber (BEBC), was achieved submerging the magnet in a saturated bath of stagnant helium at atmospheric pressure and 4.2 K temperature. Heat transfer in these conditions is associated to phase transition from liquid to vapour, the boiling process. The heat flux transferred from the heated surface to the helium in boiling regime has a complex but known behaviour, shown schematically in Fig. 17.

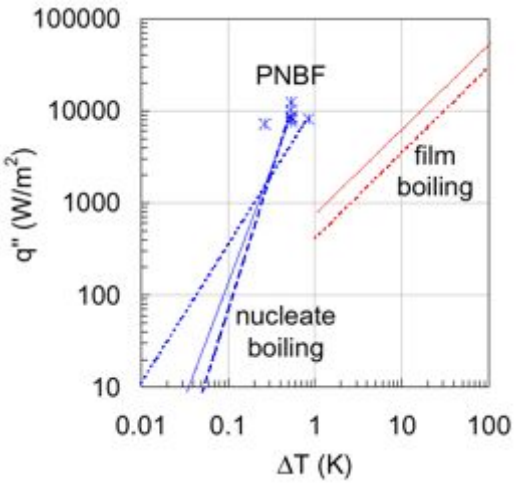

Figure 17. Heat flux for boiling heat transfer regimes. The transition between nucleate and film boiling conditions is unstable.

We report there a collection of results of correlation fits to measured heat flux data as a function of the temperature difference between the heated surface and the bulk of the bath [6, 7]. If the temperature difference is small heat transfer takes place in the nucleate boiling regime, where the heat transferred is proportional to approximately the third power of the temperature difference. For temperature differences in the range of 0.5 K the heat transfer reaches a crisis point at which conditions become unstable. The maximum heat flux that can be reached is the Peak Nucleate Boiling Flux (PNBF) that depends on the nature and heated surface. Material, surface roughness, surface coating, surface orientation with respect to gravity can affect the heat transfer and PNBF by a factor 2 [8]. The value of the PNBF for helium, however, has never been found to exceed 10 kW/m^2. Increasing the heat flux above the PNBF the surface covers with a film of vapour and the heat transfer degrades. This regime is called of film boiling and is characterised by a linear dependence of the heat flux on the temperature difference. Transition from nucleate to film boiling and back is hysteretic, takes place at constant heat flux and is characterised by a sudden jump in the temperature difference at the surface.

From the typical data of Fig. 17 it is possible to calculate an effective heat transfer coefficient h as the ratio of heat flux to temperature difference ΔT between the heated surface at temperature T_s and the helium at temperature T_{he}. This has been done below, leading to the following approximate expressions:

$$h_{Nucleate} = 405 + 37 \cdot 10^3 \left(T_s - T_{he}\right)^{1.4} \tag{23}$$

$$h_{Film} = 592 \left(T_s - T_{he}\right)^{-0.077} \tag{24}$$

that hold for saturated helium at atmospheric pressure. The result of the expressions above is shown in the compilation of Fig. 18, together with other heat transfer mechanisms discussed later. Nucleate boiling regime is associated with extremely high values of h, changing rapidly and ranging from few hundreds of W/m^{2}K to well above 10 kW/m^{2}K for a temperature difference of 0.5 K. As soon that the PNBF is reached, however, the equivalent heat transfer drops to a constant value of the order of 400 to 600 W/m^{2}K.

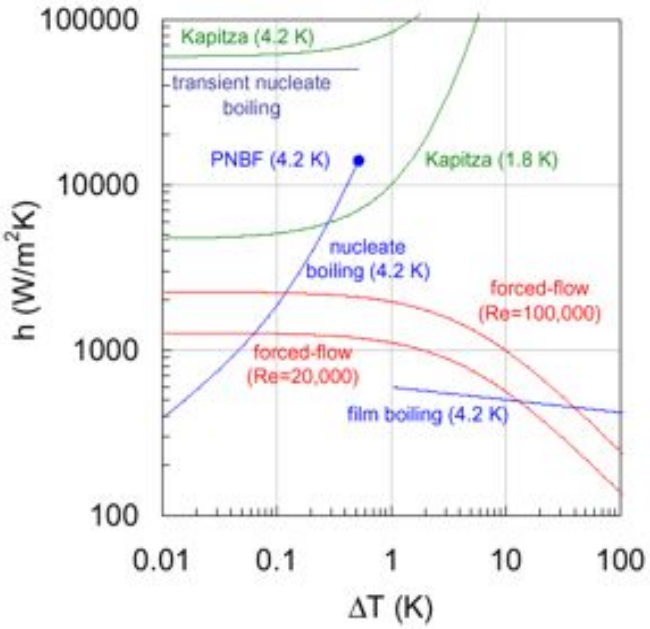

Figure 18. Summary of the equivalent heat transfer coefficient for different heat transfer regimes in helium.

During transient processes of interest for stability the heat transfer to a bath of saturated helium shows some substantial difference with respect to the steady state behaviour discussed above. It is found in particular in measurements that the nucleate boiling persists at much higher heat fluxes than those observed in steady state conditions, more than one order of magnitude higher than the PNBF discussed above. This is the effect of the thermal diffusion in the helium in direct contact with the heated surface [9]. The heat transfer crisis is reached in transient condition when the helium volume affected by thermal diffusion has absorbed an energy equivalent to the latent heat of evaporation, at which point the transition to film boiling takes place. Also the equivalent heat transfer coefficient during transient boiling can reach extremely high values, of the order of 50 kW/m^{2}K, probably limited by Kapitza resistance at the solid wall [9].

5.2 Forced-flow

Steady-state heat transfer to a turbulent forced-flow of supercritical helium appears to be well approximated by a correlation of the Dittus-Boelter form, as shown by Yaskin [10] and Giarratano[11]. A best fit of the available data is obtained with the following expression that includes a corrections for large temperature gradients at the wetted surface:

$$h_{DB} = 0.0259 \frac{K_{He}}{D_h} \mathrm{Re}^{0.8} \mathrm{Pr}^{0.4} \left(\frac{T_{he}}{T_s} \right)^{0.716} \tag{25}$$

Steady state forced flow heat transfer for common Reynolds number in cable cooling pipes (few 10^4 to 10^5) is usually of the order of 1000 W/m^{2}K. A large temperature difference, several K, between the heated surface and the bulk causes an appreciable degradation of the above values, as shown in Fig. H2.

As for boiling conditions, strong variations of the heat transfer are observed during fast transients. Giarratano [12] and Bloem [13] measured transient heat transfer to a forced flow of supercritical helium in dedicated measurements on short test sections (see Fig. 19).

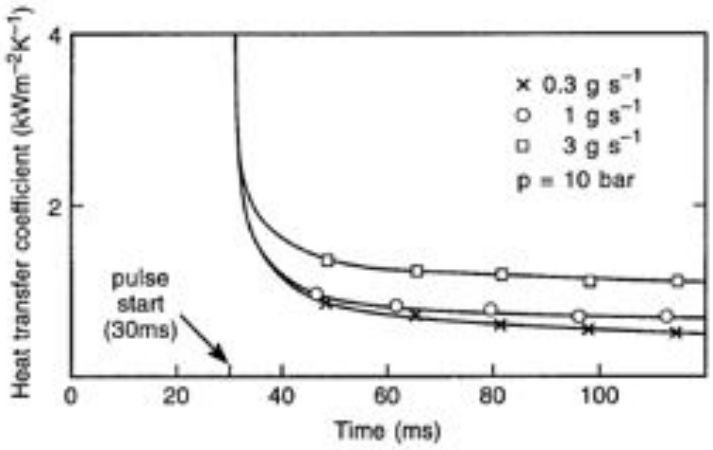

Figure 19. Transient heat transfer coefficient in supercritical helium, measured by Bloem [13]. Reprinted from ref. [13] with kind permission from Butterworth-Heinemann journals, Elsevier Science Ltd, The Boulevard, Langford Lane, Kidlington OX5 1GB, UK

The experiments showed an initial peak in the heat transfer coefficient at early times, below 1 ms. At later times, in the range of some ms to about a hundred ms, the initial peak decreased approximately

with the inverse of the square root of time. This behaviour can be explained in terms of the diffusion of heat in the thermal boundary layer. Using the analytical solution of diffusion in a semi-infinite body (the helium) due to a heat flux step at the surface, the effective heat transfer coefficient can be computed as (Bloem[13]):

$$h_{BLQ} = \frac{1}{2}\sqrt{\frac{\pi K_{he}\rho_{he}c_{he}}{t}} \tag{26}$$

where K_{He} is the heat conductivity of helium. The expression above is shown to fit properly the experimental data for times longer than a ms and until the thermal boundary layer is fully developed. At early times Eq. (26) would tend to predict an exceedingly high heat transfer coefficient, consistently with the assumptions of the analytical calculation. In reality the early values of h are found to be limited by the Kapitza resistance [14] at the contact surface of strand and, which gives a significant contribution only when the transient heat transfer coefficient is in the order or larger than 10 kW/m^{2}K (or in the case that the wetting helium is in the superfluid state as discussed later). At later times, usually around 10 to 100 ms, the thermal boundary layer is fully developed and the steady state value of h is approached. An empirical expression for the heat transfer during the transient, describing the transition from transient to steady-state conditions, can be obtained as follows:

$$h = \max\left\{h_{BLQ}, h_{DB}\right\} \tag{27}$$

giving a good agreement with the experimental results, and showing how for short pulses the heat transfer coefficient only depends on the helium state and not on the flow conditions.

During the flow transients generated by the heating induced flow the two processes are combined, i.e. the boundary layer changes in thickness during the thermal diffusion process. Experimental measurements in these conditions, and in particualr on transient heat transfer over long lengths, pose some principle problems and results are so far not available. This issue is important, as increased turbulence in the flow can contribute to the stability margin. It is not clear whether the phenomenon has a local nature or depends on the heated length and the time scales involved in the establishment of the helium expulsion from the normal zone.

5.3 Superfluid helium

Helium undergoes a quantum transition, much similar to the phenomenon of superconductivity, when it is cooled below the so called *lambda* point, i.e. 2.17 K at ambient pressure. In this state it becomes superfluid helium, characterised by very small viscosity and an exceedingly high thermal conductivity that allows removal of heat at high rates both at the surface interface with solid materials (e.g. a superconducting strand) as well as in the fluid bulk. For this reason superfluid helium is used as a coolant in high-performance magnetic systems based on NbTi or Nb3Sn, where the low operating temperature is used to boost the critical current density. An additional advantage is that the thermal conductivity of a superfluid helium bath can be used to evacuate the heat loads in the magnetic system without requiring fluid convection. The high heat transfer rate of superfluid helium can be described in relevant conditions by an internal convection of two fluid species, a normal component and a superfluid component that carries no entropy. The two species move in counter-flow to maintain total density, thus also achieving net energy transport.

In the case of normal helium considered in the previous sections, heat transfer is controlled in most situations by the vapour film (boiling heat transfer) or by the thermal resistance of the boundary layer (convection). In superfluid helium, on the contrary, the heat fluxes that can be sustained in the bulk

fluid are so large that the thermal resistance at the solid-fluid interface becomes important. The dominating mechanism for the heat resistance at the interface is the mis-match in the propagation of the phonons. This interface thermal resistance is usually called Kapitza resistance, and is in principle present at all operating temperatures. The heat flux across the Kapitza resistane can be roughly approximated by the following epression:

$$q''_{Kapitza} = \sigma\left(T_s^n - T_{he}^n\right) \tag{28}$$

where the exponent n is in the range of 3 to 4. The constant σ depends on the nature and state of the material and for a value of n of 4 its value can range from 200 to 400 W/m^{2}K^4. With this choice of n the equivalent heat transfer coefficient at the surface is then given by:

$$h_{Kapitza} = \sigma\left(T_s^2 + T_{he}^2\right)\left(T_s + T_{he}\right) \tag{29}.$$

Typical values of the equivalent heat transfer coefficeint are plotted in Fig. 18 for comparison with the other heat transfer regimes. At low temperature (below 2 K) the Kapitza resistance is relatively large, corresponding to heat transfer coefficient in the range of 5 kW/m^{2}K, and is usually the main limit for heat transfer. Already at 4.2 K, though, the equivalent heat transfer coefficient is extremely high, above 50 kW/m^{2}K, thus explaining why the Kapitza resistance is generally not a limiting factor in heat transfer to normal helium.

6 STABILIZATION STRATEGIES

6.1 Adiabatic stabilization

The lower limit for the energy margin of a superconductor can be obtained considering that the cable responds adiabatically to the external energy input. This is the case in the absence of a cryogenic cooling fluid and whenever the volume affected by the external energy input is so large that heat conduction at the boundary of the normal zone can be neglected. The absence of cooling by a stagnant or flowing cryogenic fluid, most frequently liquid helium, is typical of small windings, either either wound from a *dry* superconductor or impregnated with organic resins. Dry or impregnated windings conductively cooled using as a heat sink a cryo-cooler, are becoming increasingly attractive owing to the appeal of cryogen-free operation. Cooling happens in this type of winding on a time scale that is much longer than the time of relevance for discriminating between recovery and thermal runaway. Hence for these magnets the cooling term is absent in the heat balance. In this case the energy balance simplifies to:

$$C\frac{\partial T}{\partial t} = q'''_{ext} + q'''_J \tag{30}.$$

As expressed by Eq. (18) any excursion of the superconductor above the current sharing temperature T_{cs} will cause the appearance of Joule heating resulting in an inevitable thermal runaway[1]. The current sharing temperature provides in this case the boundary between recovery and thermal runaway. The stability margin corresponds to the energy necessary to increase the superconductor temperature from

[1] Strictly speaking, in the case of a practical superconductor with voltage-current characteristic described by the power-law relation, Joule heating is always positive, although small, even below current sharing. In this case the superconductor would never be stable even in the absence of an external energy input. The steady state Joule heating is however small and is removed by the cooling system, inevitable present, that acts on times much longer than the time scales of interest for stability, but sufficient for maintaining the steady state operating temperature.

operating conditions to T_{cs}. Within the approximations considered so far this can be calculated integrating Eq. (30) taking into account that below T_{cs} the Joule heating is zero:

$$\int_0^{\infty} q'''_{ext}\, dt = \int_{T_{op}}^{T_{cs}} C\, dT \tag{31}.$$

The integral on the l.h.s of Eq. (31) corresponds to the energy margin, while the integral on the r.h.s is the difference of volumetric specific enthalpy between operating temperature and current sharing temperature. We can thus write that for an adiabatic superconductor the energy margin is:

$$\Delta Q''' = H(T_{cs}) - H(T_{op}) \tag{32}$$

with the definition:

$$H(T) = \int_0^{T} C(T')\, dT' \tag{33}.$$

For this reason the mechanism underlying adiabatic stability, namely the heat capacity of the superconductor, is also referred to as *enthalpy stabilization*.

In order to estimate the orders of magnitude of the energy margin in adiabatic conditions it is necessary to examine the typical values of heat capacity and specific volumetric enthalpy of the typical materials present in a superconducting winding. This is done in Figs. 20 and 21 respectively. The functional dependence of the volumetric heat capacity is different among pure metals (Copper, Alluminium), alloys (stainless steel), superconductors (NbTi and Nb_3Sn) and organic composites (resin and typical insulators) because of the different weights of the electronic and phonon contributions to the specific heat. However, in spite of the large range of values, a general feature exhibited by all materials is the decrease of specific heat approaching the absolute zero. The consequence is that the enthalpy difference for a given temperature margin ΔT is smaller at lower temperature, as can be inferred taking the volumetric specific enthalpy difference for a fixed temperature interval from Fig. 21. The effect is particularly important, nearly one order of magnitude, when considering operation in superfluid helium, at 1.8 to 2 K, as compared to operation in atmospheric pressure liquid helium, at 4.2 K.

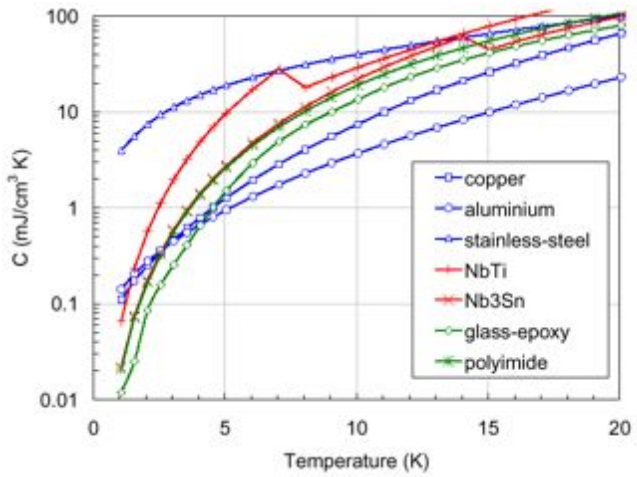

Figure 20. Volumetric heat capacity for typical materials used in low-temperature superconducting magnets.

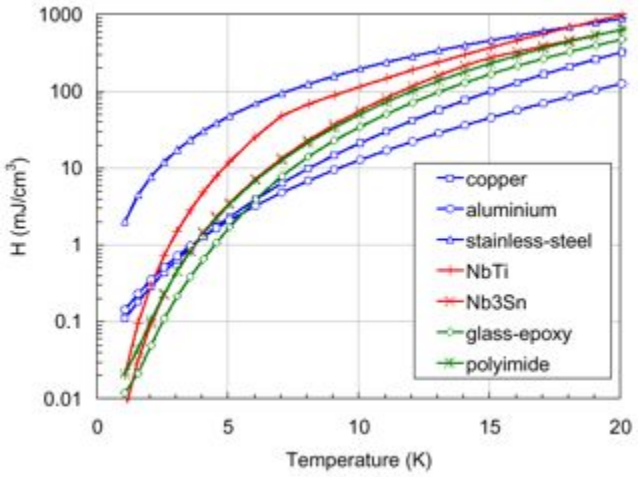

Figure 21. Volumetric specific enthalpy for typical materials used in low-temperature superconducting magnets, obtained integrating the data of Fig. 20.

The adiabatic energy margin can be estimated using the data in Fig. 21 adding the individual contributions of heat capacity of all materials participating to the temperature excursion. We can do this by taking the weighted average of the volumetric specific enthalpy:

$$\Delta Q''' = \sum f_i \left(H_i(T_{cs}) - H_i(T_{op}) \right) \tag{34}$$

where the f_i is the materials fraction of the i-th component characterised by the specific volumetric enthalpy H_i.

The energy margin in Eq. (34) depends on the operating temperature T_{op} and on the operating field B_{op} and current I_{op} through the current sharing temperature. It is hence possible to scan the energy margin over the whole operating space for a given superconductor once the material fractions are fixed. A typical strand for low termperature applications has a ratio of stabilizer to superconductor in the range of 1 to 1.5. As we have made the assumption that the external energy input is distributed over a large volume of the winding, we include in the calculation also the electrical insulation. Typical fractions of materials for impregnated windings are in the range of 30 % of superconducting material (f_{sc} = 0.3), 40 % of stabilizer (f_{st} = 0.4) and 30 % of insulation (f_{in} = 0.3).

In Fig. 22 we report the result of the calculation of Eq. (34) for NbTi and Nb_3Sn as superconducting material operating initially at a temperature of 4.2 K. The calculation has been performed for several values of the operating fields, and is plotted as a function of the operating ratio of the critical current I_{op}/I_c. We see at once the clear difference among the two materials, due to the fact that Nb_3Sn has a higher critical temperature and thus exploits a region of higher heat capacity for stabilization. Also, it is clear that approaching the limits of performance of the conductor (8 to 10 T for NbTi and 16 to 20 T for Nb_3Sn) the adiabatic energy margin for an efficient use of the superconductor (operating fraction of the critical current around 0.8) becomes extremely small (below 1 mJ/cm^3) and the magnet will not be able to withstand even the smallest perturbation without quenching.

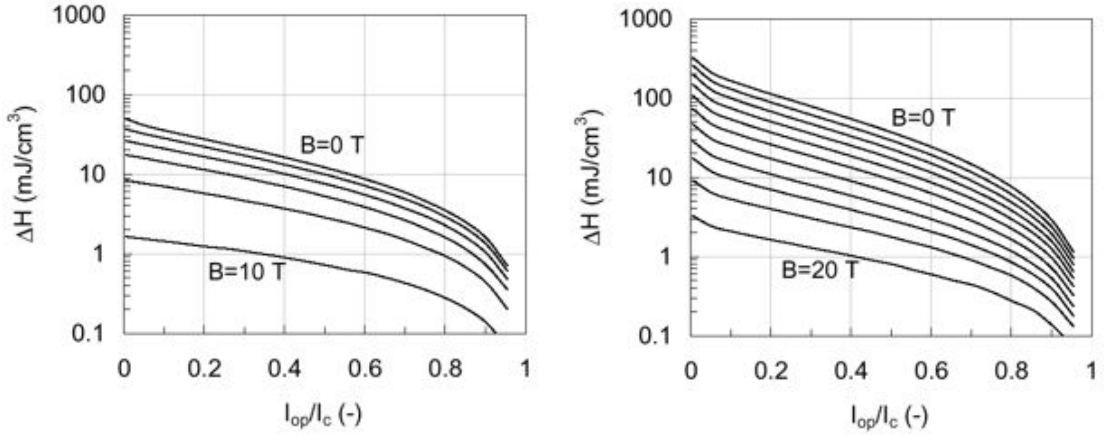

Figure 22. Adiabatic energy margin for a typical winding, with 30 % superconductor, 40 % copper and 30 % insulation, wound either using NbTi (left) or Nb_3Sn (right). The calculation has been performed with an initial operating temperature of 4.2 K, for different values of the operating field (steps of 2 T among the curves) and as a function of the ratio of operating to critical current.

Another interesting result can be obtained performing the above calxculation for different initial operating temperatures. It is in particular instructive to examine the effect of reducing the operating temperature, which is often done to raise the critical current density in the hope to increase the operating field of a magnet. The result of the calculation at 4.2 K discussed in Fig. 22 are compared in Fig. 23 to the results obtained for an initial operating temperature of 1.8 K. Because a temperature change affects the critical current, to allow a direct comparison the curves are plotted as a function of the operating current density in the superconductor. We see from the comparison of the adiabatic energy margin that subcooling has essentially no effect at low field, as in any case the dominating contribution to the energy margin is due to the heat capacity in close proximity to T_{cs}. Only at high field (8 to 10 T for NbTi and 16 to 18 T for Nb_3Sn) the effect of sub-cooling becomes appreciable. However the order of magnitude of the absolute gain in stability is at most few mJ/cm^3, at best comparable with the expected mechanical and electromagnetic perturbations in a typical magnet.

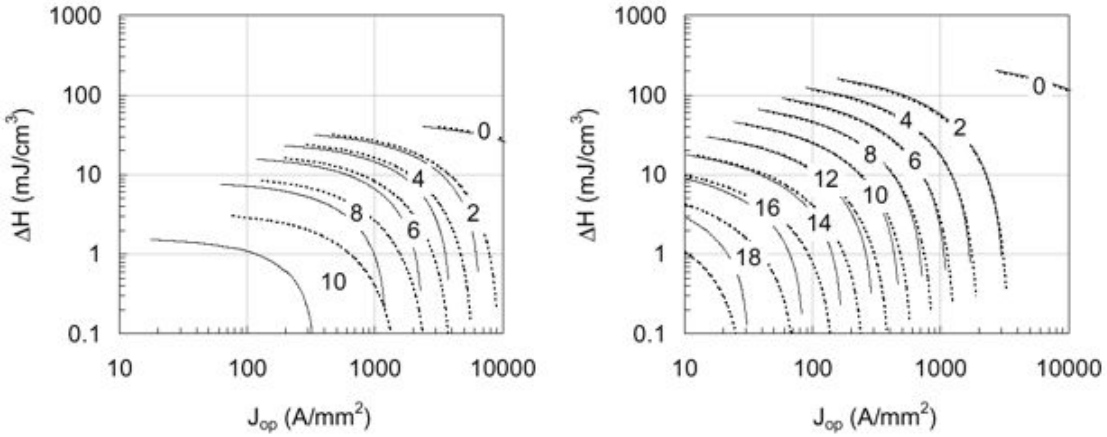

Figure 23. Adiabatic energy margin for a typical winding, with 30 % superconductor, 40 % copper and 30 % insulation, wound either using NbTi (left) or Nb_3Sn (right) and computed for an initial operating temperature of 4.2 K and 1.8 K. The calculation has been performed for different values of the operating field (steps of 2 T among the curves) and as a function of the operating current density to allow direct comparison of the results.

For the above reasons enthalpy stabilization is not sufficient to make the best use of the current carrying potential of superconductors and other means have been devised to cope with the perturbation spectrum, especially in large magnet systems.

Adiabatic stability of a MRI magnet

One of the most widespread and well known present applications of superconductivity are magnets for Magnetic Resonance Imaging (MRI). These magnets are solenoids with a very good field homogeneity and large bore, as large as 1 m diameter and 1.5 m length, to allow full-body scans of human beings. Typical field levels in the bore of the solenoid are at present in the 1 to 2 T range. For cost and maintenance reasons these magnets are built with high operating current densities, and with little or no cryogen in the winding pack. They are essentially adiabatic, and therefore they must be carefully designed to avoid training and quenches.

A typical MRI magnet winding pack is subdivided in a series of thin coaxial, possibly nested solenoids for shielding, that produce the field and correct for winding and geometrical errors. To obtain a good field homogeneity the winding geometry must be controlled and maintained tightly. In addition the contribution from the magnetisation of the superconductor must be minimised. Because of these requirements MRI magnets are generally wound from single wires with medium size superconducting filaments. The winding pack is impregnated so that it forms a single rigid unit and the wires are constrained in position. Cooling is indirect, by conduction through the winding pack. The thin winding pack allows heat removal under a small temperature gradient.

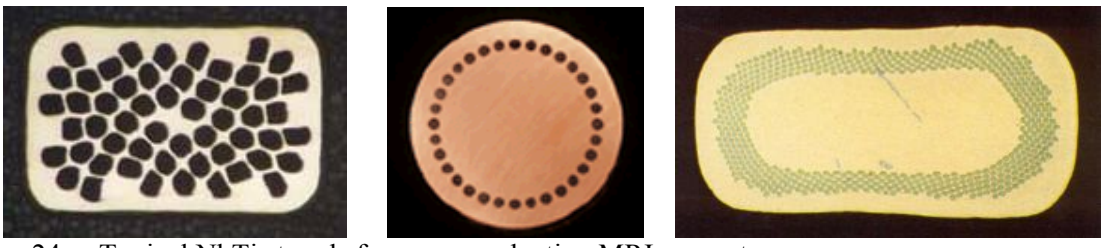

Figure 24. Typical NbTi strands for superconducting MRI magnets.

A typical MRI magnet is wound with NbTi wire, well adapted to the field range required, of the types shown in Fig. 24. The wire has a high Copper:NbTi ratio, of the order of 5 to 10, mostly for protection reasons because of the large inductance of the coil. Wires for MRI magnets are produced with round or rectangular shape (to ease winding), and have external dimensions of the order of 1 to 2 mm. The NbTi filaments have typical diameter of 50 μm. At low field they are delivered with a guaranteed critical current density in the NbTi cross section in the range of 5000 A/mm^2. These must be compared to operating current densities in the range of 200 A/mm^2 in the strand, i.e. of the order of 1000 to 2000 A/mm^2 referred to the NbTi cross section. We see at once that MRI magnets are designed with large operating margins to increase their reliability. Still, additional care is necessary.

In the adiabatic case we can estimate the stability margin as the enthalpy of the wire from operating conditions to the current sharing temperature. To do this we take in account the contribution of copper, the main component in the wire, and NbTi and we use the diagram reported in Fig. 21. Assuming an operating temperature of 4.2 K, and a current sharing temperature of 7.5 K (consistent with the operating current and field range given above) the 3.3 K temperature margin corresponds to an enthalpy change of 6.14 mJ/cm^3 for copper and 46.7 mJ/cm^3 for NbTi. The total adiabatic energy margin is obtained using the weighted sum of Eq. (34) and gives approximately 13 mJ/cm^3. This value is larger than our estimate of the energy release due to movement of the conductor, but does not leave much contingency to cope with uncertainties in the actual temperature margin and other possible energy inputs. Resin impregnation of the winding pack, as mentioned previously, is common practice

to avoid movements and thus to minimise the energy release through wire motion. Note that cracking of the impregnation resin during cooldown and energization - resins have large thermal contraction from room temperature to 4.2 K, but little tensile strength at cryogenic temperatures - can also be a source of localised energy release. This is generally avoided by filling void volumes in the winding pack with fillers and fibre cloths or ropes that increase the tensile strength.

6.2 Cryostability

Early superconducting coils had a wide spectrum of large perturbations, significantly above the summary presented in Fig. 5. This was either because the strands and tapes used were prone to flux jumping, or because the mechanic design was not adapted to avoid movements, slips, insulation cracks and the associated energy releases during energization. The adiabatic energy margin, as discussed in the previous section, was by no means sufficient to accommodate the energy perturbations. A small and localised normal zone had in addition no chance to recover, because the Joule heating of the superconducting material in normal state was extremely high, and therefore the coils quenched prematurely. Based on this observation, Krantowitz and Stekly [15] and Stekly and Zar [16] added a high electrical conductivity shunt backing the superconductor, a pure copper *stabiliser*, and exposed this material to a liquid helium bath of large volume and thus constant temperature. The effect was dramatic, improving the performance of the magnet and paving the way to large size applications of superconductivity.

This result was achieved thanks to two beneficial effects: on one side the Joule heat generation in case of transition was largely decreased by the stabilizer, while on the other side the superconductor was efficiently cooled through boiling heat transfer. Cryogenic stabilisation, or *cryostability*, was achieved when the steady state composite temperature that would be attained with the full operating current flowing in the stabiliser was below the critical temperature of the superconductor. In this case the initial normal zone, caused by an arbitrary energy source, would shrink and eventually disappear.

The cryostability condition can be best understood taking again the 1-D heat balance of Eq. (7). As the cryostability condition applies independently on the length of the conductor subjected to an energy perturbation, we can neglect the heat conduction term, and we obtain:

$$C\frac{\partial T}{\partial t} = q'''_{ext} + q'''_J - \frac{wh}{A}\left(T - T_{op}\right) \tag{35}$$

where we have made use of the fact that the helium temperature remains constant, equal to the initial operating temperature. To achieve cryostability we are seeking the condition for which in steady state, after the end of the energy pulse, the heat generated by the normal zone is equal or smaller than the heat removal at its surface. The cryostability condition is hence obtained when:

$$q'''_J \le \frac{wh}{A}\left(T - T_{op}\right) \tag{36}.$$

For the Joule power we take the linear approximation of Eq. (18), that reaches the maximum given by Eq. (15) when the superconductor is at the critical temperature. Assuming for the moment a constant heat transfer coefficient, corresponding to a linear increase of the heat flux with temperature, we obtain that the cryostability condition is given by:

$$\frac{\eta_{st}}{wA_{st}} I_{op}^2 \le h\left(T_c - T_{op}\right) \tag{37}.$$

Cryostable operation is obtained when Eq. (37) is satisfied, while in case of higher generation or smaller cooling than implied by Eq. (37) the superconductor is not cryostable. To class the mode of operation Stekly has introduced a dimensionless coefficient α defined as[16]:

$$\alpha = \frac{\eta_{st} I_{op}^2}{hwA_{st}\left(T_c - T_{op}\right)} \tag{38}.$$

Operation is cryostable for $\alpha \leq 1$, and the maximum operating cryostable current, I_{Stekly} is given by:

$$I_{Stekly} = \sqrt{\frac{hwA_{st}\left(T_c - T_{op}\right)}{\eta_{st}}} \tag{39}.$$

The cryostability condition expressed by Eqs. (37) and (38) has a simple graphical interpretation shown in Fig. 25 obtained tracing the heat generation and the heat removal per unit of cooled conductor surface as a function of operating temperature. In the case of the curve marked as (a) in the plot, the operation is cryostable as in any point heat generation is smaller than heat removal. The limiting condition is reached with the curve marked as (b), where heat generation exactly matches cooling at the critical temperature. Cryostability is violated in the case of the curves marked with (c) and (d), for which a sufficiently large perturbation will raise the superconductor temperature to a region where the heat generation exceeds cooling, thus leading to an instability. Note that once the cooling condition has been selected, it is the heat generation curve that varies with the design changes, while the heat flux to the helium is a constant.

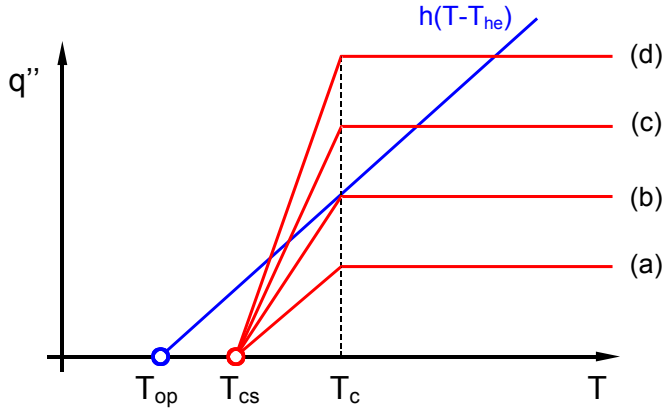

Figure 25. Graphical interpretation of the cryostability condition, in the case of constant heat transfer coefficient between the superconductor and the coolant. The graph is obtained plotting the heat generation and the removal per unit of cooled conductor surface. Several values of heat generation have been plotted (a) in the cryostable region , (b) at the cryostable limit, (c) and (d) not cryostable.

In reality the heat transfer depends strongly on the cooling conditions, as discussed earlier. In the case of boiling helium the typical heat flux is shown in Fig. 17. The equivalent heat transfer coefficient h is non-linear, with initially high values (typically 1000 to 10000 W m^{-2} K) in the nucleate boiling regime and drops to a minimum of the order of 500 W m^{-2} K at the onset of film boiling. The cryostability condition formulated above is fullfilled when under any conditions the heat removal is larger than the heat generation, that is when the maximum possible heat generation is smaller than the minimum possible heat removal. This situation is shown in Fig. 26 for the curves marked with (a) and (b). The equivalent Stekly criterion in the case of variable heat transfer is obtained taking for h the minimum

value along the boiling curve. As for the case of Fig. 25, curves (c) and (d) in Fig. 26 violate the cryostability condition. Note however that intermediate stability conditions at higher heat generation than allowed by cryostability could exist. Taking as an example curve (c) in Fig. 26, we see that under small perturbations (small temperature increase) the heat removal is still larger than the generation. A conductor operating in this condition would therefore recover from sufficiently small energy inputs, but it would be unstable for large enough energy depositions.

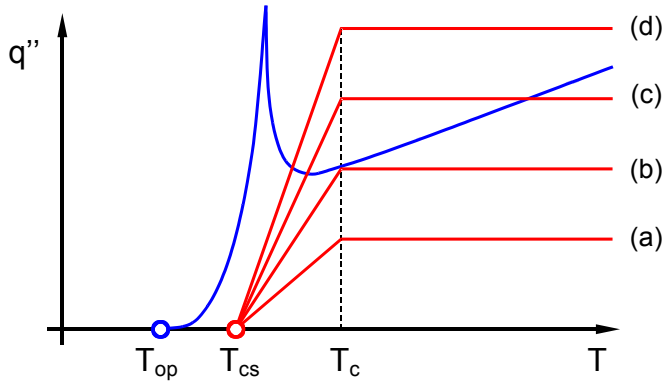

Figure 26. Graphical interpretation of the cryostability condition, in the case of boiling heat transfer between the superconductor and the coolant. Cryostabilty is obtained for the curves marked (a) and (b), but not for the generation curves marked as (c) and (d).

Cryostability: the BEBC magnet

Cryostable magnets were among the first to be built soon after the formulation of this principle, in the early 70's. A dramatic example was the Big European Bubble Chamber (BEBC) at CERN [17], a 4.7 m bore split solenoid with a 0.5 m gap producing a maximum field in its centre of 3.5 T, corresponding to a maximum field at the conductor of 5.1 T, and storing an energy of 800 MJ (see Fig. 27).

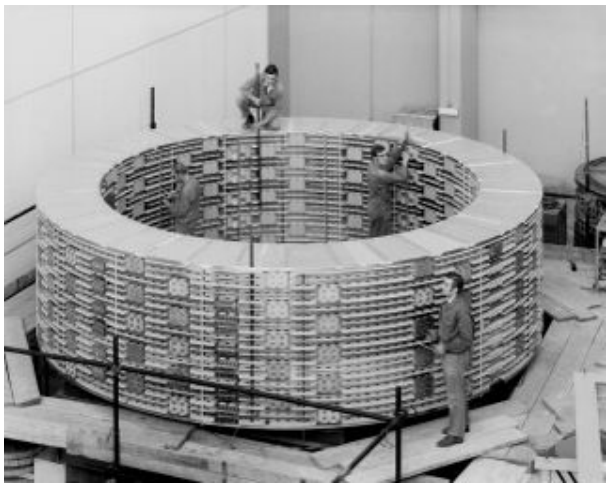

Figure 27. One of the two coils forming the BEBC split-solenoid magnet at CERN.

Each coil was wound in 20 pancakes out of a flat monolithic conductor with 3 mm thickness and 61 mm width, schematically shown in Fig. 28. This conductor was itself a composite containing 200 untwisted NbTi filaments with a diameter of about 200 μm in an OFHC copper matrix. The conductor had a total NbTi area of approximately 6.5 mm^2, and about 176.5 mm^2 of copper cross section. The

nominal operating current of the conductor was 5700 A, corresponding to an operating current density in the composite of about 30 A/mm^2. Adjacent conductors in a pancake were separated by insulation and by a copper spacer that allowed helium to wet the outer surface of the composite. Only one broad face of the composite was wetted (the other face was pressed against the insulation and a reinforcing steel strip), thus resulting in a wetted perimeter of 61 mm.

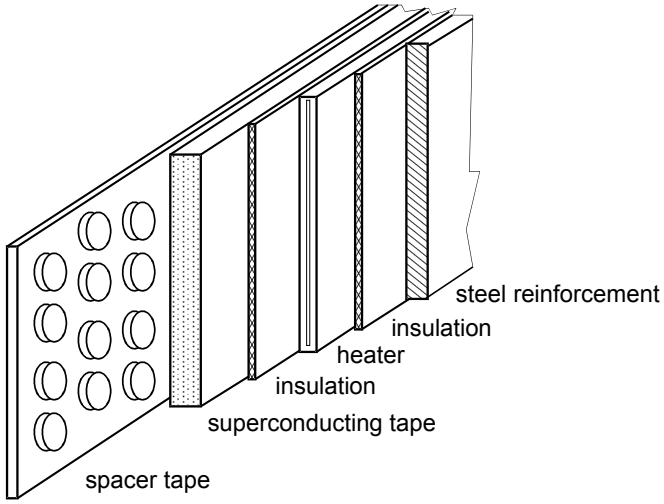

Figure 28. Schematic view of the composite structure of the BEBC conductor

In order to estimate the cryostability condition we take for boiling helium cooling, at 4.2 K, the average characteristics derived from Fig. 17 and given by Eqs. (H1) and (H2). The minimum heat transfer coefficient is of the order of 600 W/m^2 K^1. In a field of 5 T copper has an electrical resistivity of approximately 3.4 × 10^{-10} Ω m, while NbTi has critical temperature of the order of 7.4 K With these values the Stekly parameter α is 0.55, i.e. the conductor operated largely in the cryostable regime. This situation is shown in Fig. 29 that compares the heat removal and heat generation.

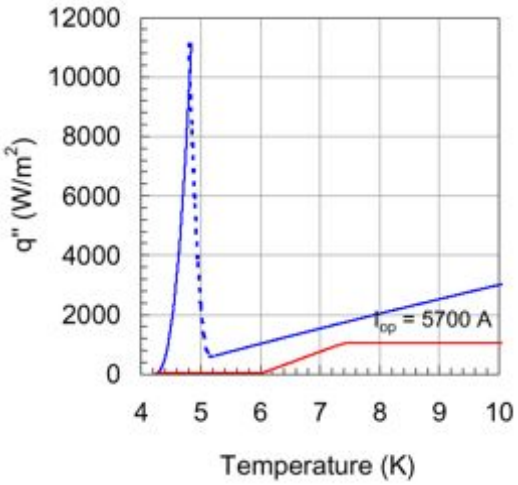

Figure 29. Plot of the heat generation and heat removal per unit cooled surface of the BEBC conductor in nominal operating conditions. The conductor is cryostable as in all possible conditions the heat removal largely exceeds generation.

Indeed the BEBC coil could be energised up to the operating current without problems, in spite of the fact that the NbTi filaments were larger than the maximum size stable against flux jump. In fact, because the filaments were not twisted in the composite, even larger magnetisation was associated with the currents that flowed in the electromagnetically coupled filaments, excited by the field ramp.

Owing to the cryostable operating regime it was possible to suppress the large magnetisation produced by these coupling currents using heaters that temporarily quenched the conductor. The conductor recovered as soon as the heaters were switched off, a rather bizarre use of cryostability.

6.3 Cold-end recovery

So far all discussions have concerned a portion of superconductor long enough to neglect all end effects. In reality perturbations happen often over finite lengths. We should hence expect that condition at the end of the resulting normal zone could help in cooling and thus provied additional stability. Stability analysis in these conditions becomes a complex matter. Still a very simple and elegant treatment was found by Maddock, James and Norris [18] that identifies steady-state equilibrium conditions taking into account the effect of heat conduction along the superconductor. The situation examined is the case of a superconducting wire with a normal zone in the center at a temperature T_{eq}, exchanging heat with a helium bath at constant temperature and sufficiently long that the two ends of the wire are at equilibrium temperature T_{op} with the coolant. Heat is transported by conduction from the normal zone (the warm end) to the extremity (the cold end). The temperature distribution along the wire is shown in Fig. 30, together with the corresponding heat generation and removal. Only one half of the wire is plotted because of the symmetry assumed.

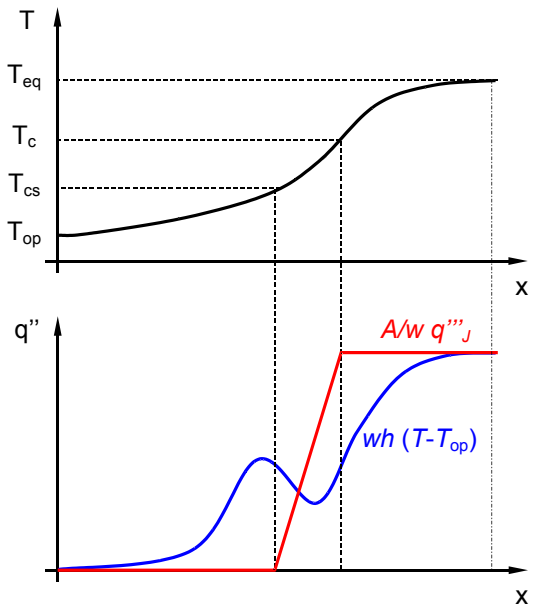

Figure 30. Temperature distribution and corresponding Joule heat generation and cooling plotted as a function of the length for a superconducting wire with a normal zone in the center. Only half of the wire length is shown because of symmetry

The heat balance in this condition is given by Eq. (7) where in principle all terms must be retained. If we seek for the equilibrium condition, however, the heat balance simplifies to:

$$q'''_J + \frac{\partial}{\partial x}\left(k\frac{\partial T}{\partial x}\right) - \frac{wh}{A}\left(T - T_{he}\right) = 0 \qquad (40).$$

Maddock and co-workers introduced a new variable S defined as:

$$S = k\frac{\partial T}{\partial x} \tag{41}$$

that represents the heat flux along the superconductor. *S* has the property that

$$\frac{\partial S}{\partial x} = \frac{\partial S}{\partial T}\frac{\partial T}{\partial x} = \frac{S}{k}\frac{\partial S}{\partial T} \tag{42}.$$

We can substitute the relation (41) in the steady state heat balance of Eq. (40) and we obtain the following relation:

$$k\left[\frac{wh}{A}\left(T - T_{he}\right) - q'''_J\right] = S\frac{\partial S}{\partial T} \tag{43}.$$

Equation (43) can be integrated directly, yelding to the following integral relation between heat generation by Joule heating and cooling:

$$\int_{T_{op}}^{T_{eq}} k\left[\frac{wh}{A}\left(T - T_{he}\right) - q'''_J\right] = \int_{S_{op}}^{S_{eq}} S\,dS \tag{44}.$$

If we now make the assumption that the normal zone is sufficiently long to have reached the equilibrium condition, so that T_{eq} given by:

$$T_{eq} = T_{op} + \frac{Aq'''_J}{wh} \tag{45}$$

then heat conduction will be zero both at the warm and at the cold end, and the relation between heat generation and cooling (for constant heat conductivity) will be simply:

$$\int_{T_{op}}^{T_{eq}} \left[h\left(T - T_{he}\right) - \frac{A}{w}q'''_J\right] = 0 \tag{46}.$$

Equation (46) is the so called *equal area theorem* and states that for equilibrium no net area should be enclosed between the heat generation and cooling curves plotted as a function of temperature. This very interesting result can be examined graphically on the same representation used in Figs. 25 and 26 to determine cryostability, and shown in Fig. 31 for the two cases of linear and boiling heat transfer. The point at temperature T_{eq} corresponds to the intersection of the generation and cooling curves. The generation curve reported, although not cryostable, is still an equilibrium condition as the area enclosed between generation and cooling is zero. The excess heat generation in the normal region is compensated by excess cooling in the superconducting region. Heat conduction functions as the vector of this heat from one region to the other.

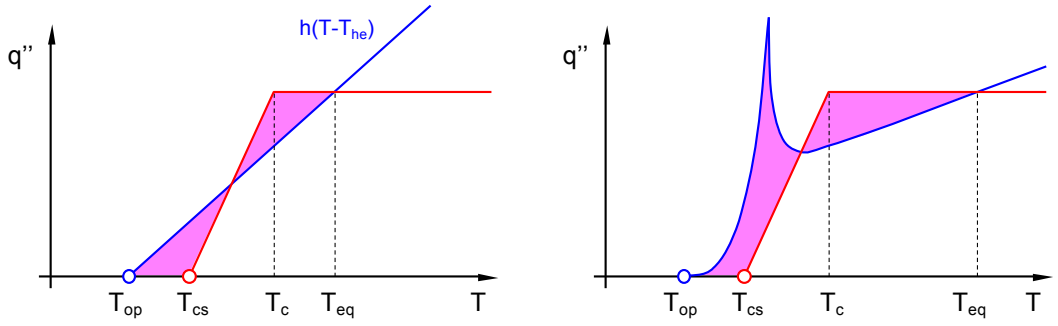

Figure 31. Graphical interpretation of the equal area condition, in the case of constant heat transfer coefficient between the superconductor and the coolant (left) and in case of boiling heat transfer (right). A superconductor characterised by the heat generation curves plotted is stable, although the cryostability condition is violated, as the net area enclosed between the generation and cooling is zero.

For the linear heat transfer case, with constant h, it is possible to determine the value of the operating current that correspond to the equal area condition. To do this we note that the equilibrium condition corresponds to the situation in which we have:

$$T_{eq} - T_c = T_{cs} - T_{op} \tag{47}$$

that derives from the similarity of the two shaded triangles in Fig 31. From Eq. (45) we also have that the equilibrium temperature is given by:

$$T_{eq} = T_{op} + \frac{\eta_{st} I_{op}^2}{whA_{st}} \tag{48}.$$

We can combine Eqs. (47) and (48) to obtain the operating current $I_{Maddock}$ corresponding to stable operation under the equal area condition:

$$I_{Maddock} = \sqrt{\frac{hwA_{st}\left[\left(T_c - T_{op}\right) + \left(T_{cs} - T_{op}\right)\right]}{\eta_{st}}} \tag{49}.$$

As expected, this current is higher than the cryostable current I_{Stekly} given in Eq. (39), implying that the superconductor can be used more effectively than limited by cryostability. The value of the Stekly parameter for operation in equal area condition is given by:

$$\alpha = 1 + \frac{\left(T_{cs} - T_{op}\right)}{\left(T_c - T_{op}\right)} \tag{50}$$

that approaches the value 2 for operation at a small fraction of the critical current (when $T_{cs} \approx T_c$). In reality the temperature variation of thermal conductivity and the non-linear character of the heat transfer can cause significant variations from the limits above, with a net effect that in general is towards higher stable operating current and corresponding Stekly parameter.

Equal area condition for the BEBC magnet

In the case already examined above for the BEBC solenoid we have computed the value of the nominal heat generation and cooling, and verified that the BEBC magnet was operating in cryostable regime. It is possible, using the same assumptions, to estimate the maximum operating current that could have been achieved in steady state stable conditions as dictated by the equal-area theorem. Of course, a change in operating current would result in a simultanous change in the produced magnetic field, of the critical properties of the NbTi superconductor, and of the copper resistiviyt. Linearising the properties in the vicinity of the nominal working point, we make the following approximations:

magnetic field at the conductor:

$$B_{op} = 0.9 \cdot 10^{-3} I_{op} \quad [T]$$

critical temperature:

$$T_c = 7.4\left[1 - \frac{B_{op} - 10.8}{5.1 - 10.8}\right] \quad [K]$$

critical current:

$$I_c = 13000\left[1 - \frac{B_{op} - 10.8}{5.1 - 10.8}\right] \quad [A]$$

from which it is possible to compute the current sharing temperature at any working conditions.

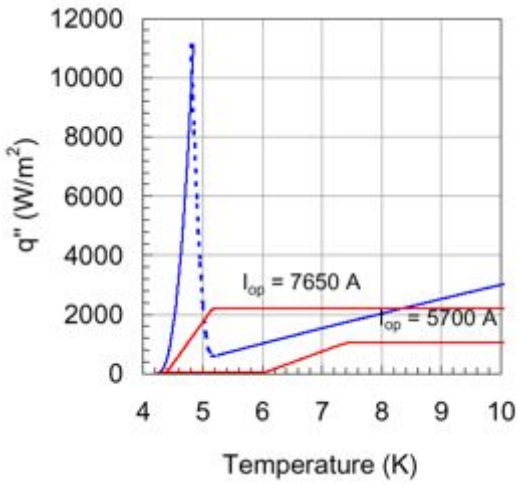

Figure 32. Equal area condition for the BEBC magnet as compared to the cryostable operating condition discussed earlier.

We can now take the same heat transfer curve as used in Fig. 29 and vary parametrically the current I_{op} until the equal area condition is reached. This situation is shown in Fig. 32. The corresponding values of the operating current is approximately 7650 A, for an operating field of 6.84 T. Ideally, this should have been the upper limit for stable steady state operation of the BEBC magnet.

The equal area condition guarantees stable operation at a current above the cryostability limit even in the case of a large portion of the winding going normal. This allows the designer to increase the

allowable operating current density with a beneficial reduction in the amount and cost of superconductor and stabilizer used for the coil construction. In fact, once established, the temperature profile obeying to the equal area theorem is stable. If we take the example of the central point, and we refer to the plot of the generation and cooling fluxes of Fig. 31, a small temperature increase will cause the cooling to become larger than generation and the conductor will evolve back to the equilibrium temperature. For a small temperature decrease the cooling will be less than the generation and the temperature will increase back up to the balance point. In last analysis the equal area theorem guarantees that the coil will suffer from no thermal runaway whatever the energy input[2], but, as for the cryostability condition, it does not quantify the energy margin of the conductor. Because in addition both cryostability and equal-area conditions apply to a long length of superconductor initially brought into normal conditions, the energy margin for a conductor operating in these conditions is in practice much larger than any perturbation expected during operation, i.e. *infinite* from an engineering point of view.

6.4 Well-cooled operation of CICC's

We have assumed so far that the cooling takes place in a helium bath, providing an ideally infinite heat sink. For some applications it is advantageous to cool the superconductor by a forced flow of helium, in which case the amount of helium available for stabilization is no longer infinite. Various superconductor configurations have been developed around this concept, of which the most successful from the stability point of view is the Cable-in-Conduit Conductor (CICC). The development of CICC's was largely motivated by the observation that cryostable pool boiling magnets (i.e. satisfying the Stekly criterion) are known to have low operating current density, and thus high size and cost. It was also clear however that large size magnets operating in a mechanic or electromagnetic noisy environments (for instance operating in rapidly changing magnetic fields or subject to significant stress cycles) require a minimum energy margin to withstand typical perturbations which cannot be absorbed adiabatically in the small heat capacity of the conductor.

Helium is the only substance known to have a large heat capacity at the low temperature. This is shown in Fig. 33, reporting the volumetric heat capacity (the product of density and specific heat at constant pressure) for different values of pressure in supercritical regime. Comparing the values of Fig. 33 to those for solid materials in Fig. 20 we see that helium can provide a heat capacity 2 to 3 orders of magnitude larger than the solid materials in the range of 4 to 10 K that is typical for low-temperature superconductors. The volumetric enthalpy is shown in Fig. 34 and also demonstrates by comparison to Fig. 21 the large heat sink that could be provided by helium.

[2] In reality for large enough energy inputs the temperature of the superconductor can become sufficiently large that the stabilizer resistivity, assumed constant so far, starts increasing sensibly. This condition however requires large energies and is not relevant for the discussion.

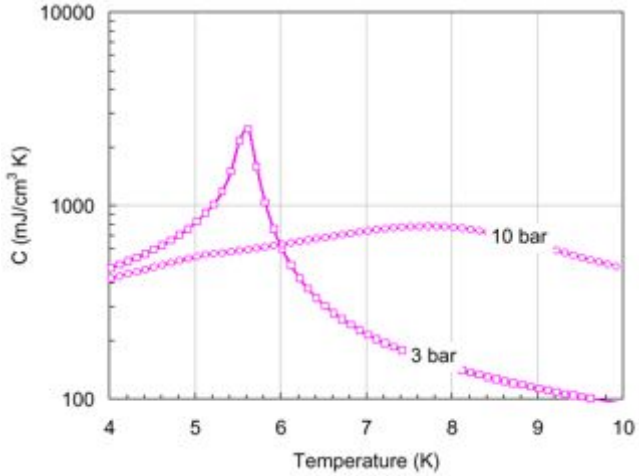

Figure 33. Volumetric heat capacity of helium at different pressures. The peak corresponds to the crossing of the pseudo-critical line in supercritical regime.

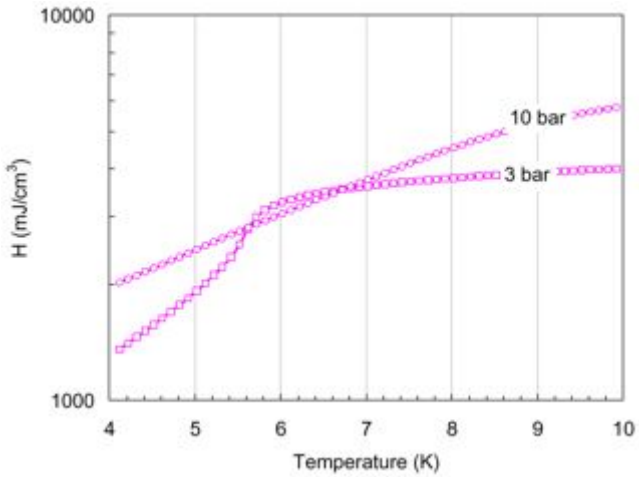

Figure 34. Volumetric specific enthalpy for helium at different pressures in supercritical regime.

The key idea behind the CICC was hence to give access to the large heat sink represented by the helium amount in the cooling circuit of the cable, thus increasing substantially the adiabatic energy margin discussed previously. At the same time the aim was to increase the heat transfer from the superconductor to the helium, so that the cryostability limit would be pushed to higher current densities.

The CICC concept evolved from the Internally Cooled Superconductors (ICS) which had found applications in magnets of considerable size between the late 60's and early 70's (see in particular the work of Morpurgo[19]). In ICS's the helium is all contained in the cooling pipe, very much like standard water-cooled copper conductors. The conductor can be wound and insulated using standard technology and the magnet is stiff both mechanically and electrically, a considerable advantage for medium and large size systems requiring, with the increasing stored energy, high discharge voltages. A control of the heat transfer and cooling conditions is achieved using supercritical helium, thus avoiding the uncertainties related to a flowing two-phase fluid. A major drawback of this concept, however, was the fact that in order to achieve good heat transfer (and thus stability and high operating current density) the helium would theoretically have to flow in the early ICS's layouts at astronomic flow rates. The advantage of the increase of the wetted perimeter obtained by subdivision of the strands was clear already at the beginning of the development of ICS (Chester [1]). Hoenig [20-22] and Dresner [23-25] developed models for the local recovery of ICS's after a sudden perturbation,

where they found that for a given stability margin the mass flow required would be proportional to the 1.5^{th} power of the hydraulic diameter. This consideration finally brought Hoenig, Iwasa and Montgomery [20,21] to present the first CICC prototype idea, shown in Fig. 35.

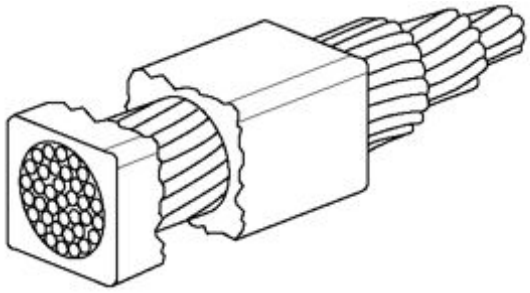

ROUND BUNDLE WITH 37 STRANDS ENCLOSED IN RECTANGULAR CONDUIT - SHOWING TRANSPOSITION OF STRANDS

Figure 35. The original concept of CICC, as presented by Hoenig, Iwasa and Montgomery [21]. Reproduced from ref. [21] by permission of Servizio Documentazione CRE-ENEA Frascati. Copyright 1975 CRE-ENEA Frascati.

Although many variants have been considered, the basic CICC geometry has changed little since. A bundle conductor is obtained cabling superconducting strands, with a typical diameter in the mm range, in several stages. The bundle is then jacketed, i.e. inserted into a helium tight conduit which provides structural support. Supercritical helium flows in the conduit within the intersticial spaces of the cable. With the cable void fractions of about 30 to 40 % achieved commonly, the channels have an effective hydraulic diameter of the order of the strand diameter, while the wetted surface is proportional to the product of strand diameter and their number. The small hydraulic diameter insures a high turbulence, while the large wetted surface achieves high heat transfer, so that their combination gives the known excellent heat transfer properties.

Strictly speaking, although it can satisfy the Stekly criterion (see later) a CICC cannot be considered as cryostable, because the amount of helium available for its stabilization (which represents the dominant heat capacity) is in any case limited to the volume in the local cross section. The consequence is that a large enough energy input will always cause a quench, a behaviour that Dresner[25,26] defines as meta-stable. The question is rather the magnitude of the energy margin $\Delta Q'''$ for a given configuration and operating condition. In the initial studies the energy input was thought to happen suddenly, and initial experiments and theory concentrated on this assumption. Throughout this section we will extend the definition to an arbitrary energy deposition time scale. Finally, in spite of the fact that the cryostability concept does not apply to CICC's, we will see that the Stekly criterion, in its original form of a power balance at the strand surface, still plays a fundamental role in its stability.

Stability in CICC's is different from the theories discussed so far because of the following reasons:

- the largest heat sink providing the energy margin is the helium, and not the enthalpy of the strands themselves or conduction at the end of the heated length;
- this heat sink is limited in amount;
- finally, the helium behaves as a compressible fluid under energy inputs from the strands implying additional feedback on the heat transfer coefficient through heating induced flow.

As a consequence, one of the the main issues in CICC stability is the heat transfer from the strand surface to the helium flow and the thermodynamic process in the limited helium amount.

Measurements of the stability margin of CICC's started early in their history [27-31]. The original idea of reducing the necessary flow in order to obtain the desired stability margin was frustrated as soon as the first experimental data were obtained: the stability margin was largely independent on the operating mass flow, as was recognized by Hoenig[28,29] (see the results reported in Fig. 36), and soon duplicated by Lue and Miller[31]. This results indicated that the heat transfer at the wetted surface of the strands during a temperature excursion was only weakly correlated to the steady state mass flow and the associated boundary layer. In later experiments, Lue, Miller and Dresner[32,33] could observe multiple stability regions both as a function of the operating current and of the operating mass fow (a typical stability margin showing the dual behaviour curve is shown in Fig. 37).

As discussed by Dresner [34] and Hoenig [30], during a strong thermal transient the heat transfer coefficient h at the strand surface changes mainly because of two reasons (see also Appendix A): (a) thermal diffusion in the boundary layer (a new thermal boundary layer is developed and thus h increases compared to the steady state value), and (b) induced flow[35] in the heated compressible helium (associated with increased turbulence and thus again an increase in h). The concurrence of these two effects explains the weak dependence of $\Delta Q'''$ on the steady mass flow and (at least qualitatively) the multivalued stability behaviour for different pulse powers.

A typical behaviour of the energy margin in CICC's was found in measurements as a function of the operating current (see the vast amount of data presented in Refs. [36] through [41]). Such a behaviour is shown schematically in Fig. 38. For sufficiently low operating current a region with high stability margin, named here after Schultz and Minervini[42] the *well-cooled* regime of operation, is observed. In this regime the stability margin is comparable to the total heat capacity available in the local cross section of the CICC, including both strands material and helium, between operating temperature T_{op} and current sharing temperature T_{cs}. At increasing current a fall in the stability margin to low values, the *ill-cooled* regime, is found. In this regime the stability margin is lower than in the well-cooled regime by one to two orders of magnitude and depends on the type and duration of the energy perturbation.

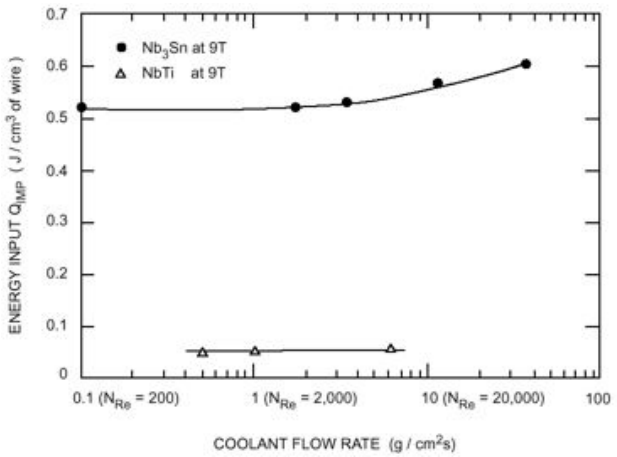

Figure 36. Energy margin of a NbTi and a Nb3Sn CICC as a function of the steady state helium flow, measured by Hoenig et al. [28]. Reproduced from ref. [28] by permission of IEEE. Copyright 1979 IEEE.

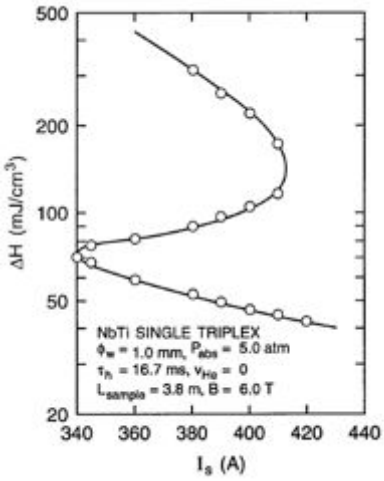

Figure 37. Energy margin of a NbTi CICC as a function of the operating current, measured by Lue et al. [33]. The experiment was performed on a single triplex CICC of 3.8 m length (L_{sample}), with strand diameter of 1 mm (ϕ_w), under zero imposed flow (v_{He}) at a helium pressure of 5 bar (p_{abs}). The backgroungd field was 6 T (B), and resistive heating took place in 16.7 ms (τ_h). Reproduced from ref. [33] by permission of IEEE. Copyright 1981 IEEE.

The transition among the two regimes was identified by Dresner[34] to be at a *limiting* operating current I_{lim}:

$$I_{\lim} = \sqrt{\frac{A_{st} wh\left(T_c - T_{op}\right)}{\eta_{st}}} \tag{51}$$

The above definition of the limiting current I_{lim} is equivalent to the Stekly criterion of Eq. (39). Equation (51) sets a condition necessary for recovery: the heat transfer from the strand to the helium must be larger than the Joule heat generation. This condition is satisfied for operating currents below I_{lim}, i.e. in the well-cooled regime. On the other hand, above I_{lim}, in the ill-cooled regime, a normal zone will always generate more heat than it can exchange to the helium, and therefore no recovery will be possible once the strand temperature is above T_{cs}.

This explains the behaviour of the energy margin below and above I_{lim}. In the well-cooled regime the recovery is possible as long as the helium temperature is below current sharing T_{cs}. Therefore the energy margin is of the order of the total heat sinks in the cable cross section between the operating temperature T_{op} and T_{cs}, including obviously the helium. In the ill-cooled regime an unstable situation is reached as soon as the strands are current sharing, and therefore the energy margin is of the order of the heat capacity of the strands between T_{op} and T_{cs} plus the energy that can be transferred to the helium during the pulse. In practical cases, the heat capacity of the helium in the cross section of a CICC is the dominant heat sink by two orders of magnitude and more, and this explains the fall in the stability margin above I_{lim}.

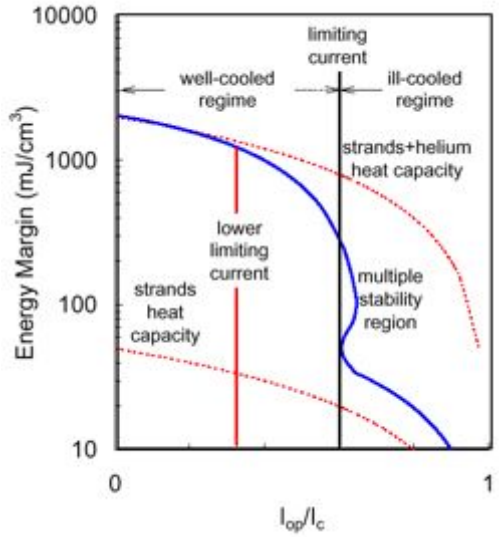

Figure 38. Schematic behaviour of the stability margin as a function of the cable operating current.

The transition between the well-cooled and ill-cooled regimes happens in reality as a gradual fall from the maximum heat sink values to the lower limit (Miller, [39]). Defining the limiting fraction i_{lim} of the critical current I_c as $i_{lim}=I=lim/I_c$, the typical extension of this fall is of the order of $(i_{lim})^{1/2}$. An intuitive explanation of this fall can be given using again the power balance at the strand surface. For the derivation of Eq. (51) it was assumed that the helium has a constant temperature T_{op}. In reality, during the transient, the helium temperature must increase as energy is absorbed, so that the power balance is displaced, i.e. power can be transferred only under a reduced temperature difference between strand and helium. Two limiting cases can be defined. The first is the ideal condition of helium at constant temperature, giving the limiting current of Eq. (51), for which however the energy absorption in the helium is negligible. Operation at (and above) I_{lim} is necessarily associated with a stability margin at the lower limit - the ill-cooled value. The second limiting case is found when the Joule heat production can be removed even when the helium temperature has increased up to T_{cs}. This second case is obtained for a current of (and below):

$$I_{\lim}^{low} = \sqrt{\frac{A_{st} wh\left(T_c - T_{cs}\right)}{\eta_{st}}} \tag{52}$$

that we call *lower limiting current* for analogy to Eq. (51) and due to the fact that $I_{\lim}^{low}$ is always smaller than I_{lim}. For operation at (and below) $I_{\lim}^{low}$ the full heat sink can be used for stabilization and the stability margin is at the upper limit - the well-cooled value. Between the two values I_{lim} and $I_{\lim}^{low}$ the stability margin falls gradually, sometimes showing the multiple stability region in the close vicinity of I_{lim}. The multiple stability region extends over a small region, which is not interesting for a safe design of a stable CICC. Therefore this feature is usually neglected.

The dependence of the stability margin on the background field B is rather obviously explained by the influence on the critical and current sharing temperatures. A higher B causes a drop both in the limiting current (through a decrease of T_c and increase of η_{st}) and in the energy margin (through a decrease in T_{cs}). Therefore, as expected, ΔE drops as the field increases. An interesting feature, however, is that the limiting current only decreases with $T_c^{1/2}$, i.e. with a dependence on B weaker than

that of the critical current. At large enough B we will always have that I_{lim} is larger than I_c and the cable will reach the critical current in well-cooled conditions.

The stability margin depends on the duration of the heating pulse, as shown experimentally by Miller et al. [31], and reported in Fig. 39. A change in the heating duration for a given energy input corresponds to a change in the energy deposition power. In the well cooled regime, i.e. for low operating currents in Fig. 39, the heat balance at the end of the pulse is in any case favourable to recovery, and therefore the energy margin does not show any significant dependence on the pulse length. When the conductor is in the ill-cooled regime, the power removal capability is limited. For short heating pulse durations the heating power increases and conductor reaches T_{cs} faster than for lower powers, corresponding to longer heating durations. Therefore the energy margin increases at increasing pulse length until it becomes comparable to the total heat capacity (as in the well cooled regime). This effect is partially balanced for very fast pulses, because the heat transfer coefficient can exhibit very high values (see earlier discussion) which could shift the well-cooled/ill-cooled transition at higher transport currents, and thus in principle higher energy margins should be expected in this range. However, the high input powers in this duration range tend to heat the conductor above 20 K, in a temperature range where the stabilizer resistivity grows quickly and the power balance is thus strongly influenced. This effect causes the saturation of the energy margin for extremely fast pulses (well below 1 ms duration).

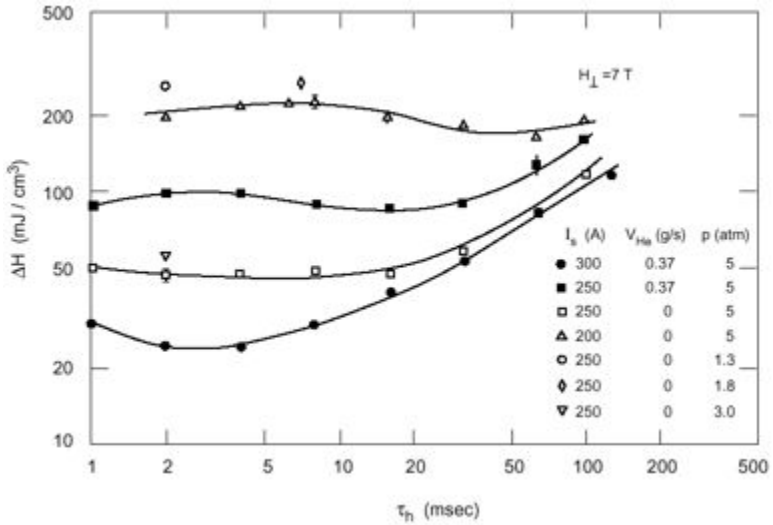

Figure 39. Dependence of the stability margin for a CICC (indicated on this plot as ΔH) on the heating time scale (τ_h), as measured by Miller et al. [31]. The parameters varied in the experiment, indicated in the inset, are the transport current in the sample I_s, the helium flow velocity v_{He} and the helium pressure p. Reproduced from ref. [31] by permission of IEEE. Copyright 1979 IEEE.

The dependence on the remaining operating conditions, typically operating temperature and pressure, is not easily quantified. The reason is that the helium heat capacity in the vicinity of the usual regimes of operation (operating pressure p_{op} of the order of 3 to 10 bar and operating temperature T_{op} around 4 to 6 K) varies strongly with both p_{op} and T_{op}. This affects both the heat sink and the heat transfer coefficient (through its transient components). An increasing temperature margin under constant operating pressure gives a higher ΔE. But a simultaneous variation of p_{op} and T_{op}, under a constant temperature margin, can produce large variation (typically of the order of a factor 2 in the range given above) in ΔE (Miller, [39]).

A mention must be made to the case that the operating point is in the superfluid helium (He-II) range. The main difference to operation in He-I is the high heat transfer capability associated with superfluid

helium. The presence of He-II has thus two effects: firstly the power balance at the strand surface is drastically changed, being displaced towards the well-cooled condition. In addition a significant heat flux leaks at the end of the heated region, thus making available a larger heat sink than the volume strictly contained in the heated region only. As an example, Lottin and Miller[41] measured the stability margin of a 2 m long conductor in an operating temperature range from 1.8 to 4.2 K. For this length the end effects are small, so that the experiment is a good basis to show the influence of the surface heat transfer.

The stability margin in the case of He-II operation behaves at low current in a way similar to what would be expected in the case of He-I operation. In fact, at low current, the current sharing and critical temperatures are well above the transition temperature T_λ from He-II to He-I (around 2 K). Heating of the strands up to current sharing implies that the surrounding helium undergoes the He-II to He-I phase transition, and the stability margin is thus governed by heat transfer in He-I. At the ill-cooled transition, however, the stability margin shows a peculiar behaviour. Owing to the large heat transfer capability in He-II, the power balance at the strand surface remains favourable for recovery as long as the wetting helium is in the He-II phase. Therefore, in a first approximation, the full heat sink between the initial operating point and the transition temperature T_λ is still available at levels of the operating current at which the conductor would have turned to be ill-cooled for operation in He-I. In other words, the conductor can still be considered as *well-cooled* for temperature excursions up to T_λ. As the helium undergoes a phase transition at the temperature T_λ, the available heat sink is significant, of the order of 200 mJ/cm^3 of helium volume. At increasing current, finally, the power balance can again become unfavourable, as soon as the heat flux limits in He-II are reached. There the final transition to the ill-cooled regime of operation takes place. This behaviour is shown in Fig. 40 following measurements of Lottin and Miller [41]

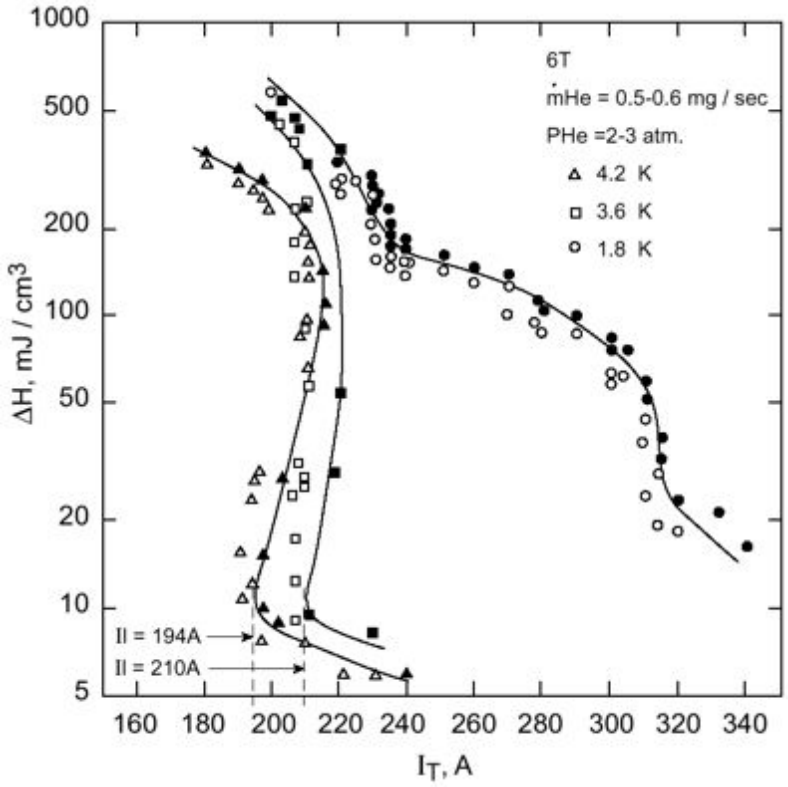

Figure 40. Stability margin of a NbTi CICC as a function of the operating current, measured by Lottin and Miller [41], at different temperatures in supercritical and superfluid helium. Reproduced from ref. [41] by permission of IEEE. Copyright 1983 IEEE.

6.5 Minimum propagating zones

The discussion so far examined normal zones extending over large lengths of superconductor, ideally as large as the whole winding length. In reality normal zones are established by small energy inputs over limited lengths of superconductor. In order to withstand these inputs the cryostability and equal-area conditions would require a much too severe limitation on the operating current density. A better design criteria can be identified resorting to the concept of minimum propagating zone originally defined by Wipf [43]. This concept was developed to a great extend by Wilson and Iwasa [44]. Following Wilson we consider again the case of a superconducting wire with a normal zone in the center. Using the auxiliary variable S representing the heat flux along the wire, because of symmetry at the center of the normal zone we must have that:

$$S = 0 \tag{53}$$

irrespective of the temperature reached by the superconductor. In this case we can use again the equal area theorem and state that an equilibrium condition is defined by Eq. (46) (neglecting the variation of the thermal conductivity with temperature) where now however the central temperature T'_{eq} is no longer T_{eq} but is rather defined as the temperature where the equal area condition is satisfied. This situation is shown graphically in Fig. 41.

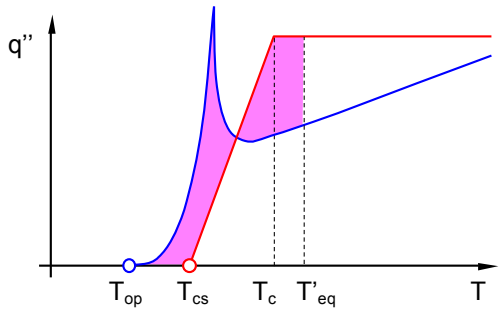

Figure 41. Graphical interpretation of the equal area theorem in the case of a heat generation above the maximum steady state allowed by the equal area theorem. The superconductor temperature profile with maximum temperature T'_{eq} is an equilibrium point as it also satisfies the equal area condition, but it is unstable.

For a choice of the heat generation above the one allowed for steady state equilibrium by the equal area theorem the central temperature T'_{eq} must be smaller than T_{eq}. The corresponding temperature profile in space can be found integrating numerically Eq. (46) in space. A family of such profiles, as produced by Wilson [44] is shown in Fig. 42. Each curve in the family corresponds to a different generation curve, and thus to a different equilibrium temperature. A property of the temperature profiles thus obtained is that for a given heat generation and cooling condition any normal zone with a temperature profile below the one obtained will collapse because the cooling exceeds the generation, and the superconductor will recover rfom the local transition. If the temperature profile of a normal zone is above the one obtained by the equal area condition, then the normal zone will grow in time leading to a thermal runaway. Hence the normal zone identified by this modified equal area condition represents an unstable equilibrium point, determining the boundary between recovery and thermal runaway. Because of this it has been called the Minimum Propagating Zone (MPZ) [43].

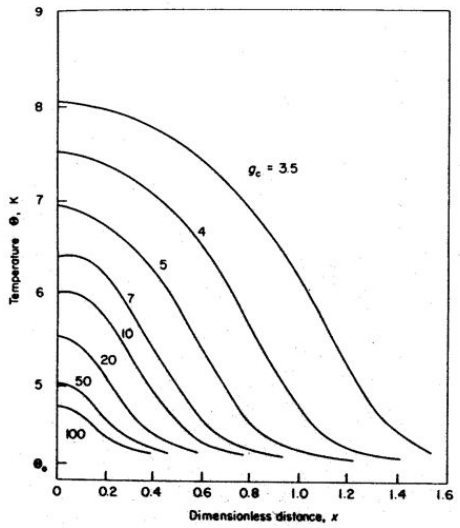

Figure 42. Family of temperature profiles corresponding to Minimum Propagating Zones obtained for different Joule heat generation conditions. Each curve represents the unstable equilibrium boundary between a recovery and a thermal runaway. Reproduced from [44].

The MPZ concept allows to have an estimate of the energy margin of the superconductor against short energy perturbations. It was observed by Wilson that if an energy input has a dimension in space smaller than the MPZ length then the temperature profile evolves quickly towards the MPZ profile. This led him to postulate that the energy margin can be estimated as the energy necessary to istantaneously establish the MPZ. This can be regarded in fact as the minimum energy necessary in all conditions to quench the conductor, or Minimum Quench Energy (MQE), and is therefore a conservative estimate for the energy margin. Any energy input happening on a finite time scale will be associated with heat transport and will result in an energy margin larger than the MQE.

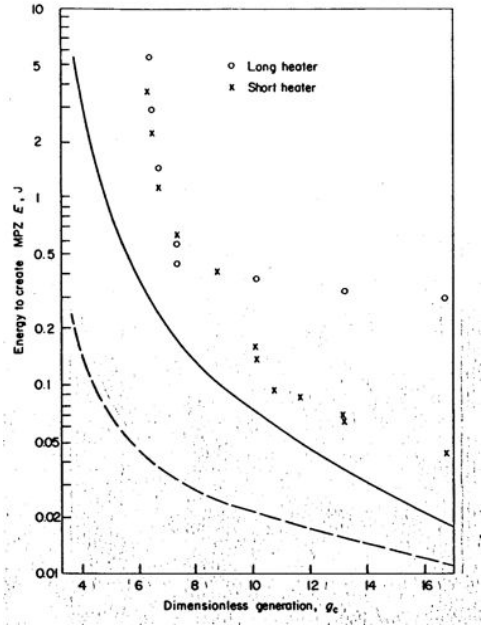

Figure 43. Measured and computed energy margin for a small solenoid equipped with heaters, plotted as a function of dimensionless Joule heat generation, after [44]. The computed curves refer to the MQE following either a 1-D or a 2-D calculation. Reproduced from [44].

Heat conduction in more than one dimension, as used to establish the heat balance, has a similar effect providing additional cooling for the MPZ. A demonstration of this is shown in Fig. 43, that reports measured energy margin vs. the result of calculations in 1-D and 2-D geometry. The agreement with the 2-D calculation is evident. Also it is clear that, as expected, the energy margin is larger than the MQE as computed from the theory above.

6.6 Transient stability in the general case

At present fully cryostable magnets are rarely the preferred designer choice. In an efficient magnet design the cable operating current density must be kept high to make the magnet cross section as small as possible. For a specified field or stored energy and thus a given magnetomotive force a maximum current density results in a decreased material and production cost. As we have shown previously a cryostable magnet needs a large amount of copper stabiliser - compared to the amount of superconductor - and a large amount of helium providing an ideally infinite heat sink. Therefore a cryostable magnet has an intrinsically low operating current density.

On the other hand, cryostability implies that the conductor is stable against *any* disturbance spectrum, independent on the magnet details and operating mode. In reality the variety of conductor designs and of magnet winding techniques, together with the variety of operating requirements, result in a wide range of possible disturbance spectra. A cryostable conductor design is therefore, in general, excessively safe. Indeed, most magnets presently designed and built are not cryostable at the operating point, but they can still be operated reliably. The common feature of these magnets is that their stability margin is above the disturbance spectrum experienced during operation. The first step in a sound design is thus to estimate the envelope of the perturbations that will be experienced. Afterwards the conductor can be designed to accommodate these perturbations by means of a sufficiently large stability margin. Note that this process can imply iterations as the disturbance spectrum can depend on the conductor and coil design itself.

Depending on the energy release dominating the disturbance spectrum the different stabilisation principles discussed in the previous sections can be used. A magnet operated in steady state mode, with a tightly packed winding, affected by small mechanical disturbances localised in time and space (e.g. in the case of fully impregnated windings) may rely on the heat sink provided by the small enthalpy margin of the superconductor and stabiliser themselves: an *adiabatic winding*. To stabilise larger perturbations the additional heat sink provided by helium may be necessary. Bringing helium in close contact with the conductor thus increases its stability margin, provided that the heat transfer at the wetted surface is efficient in the time scale of the energy deposition considered. Magnets with small amounts of added helium (or other heat sinks) are called *quasi-adiabatic* as they would in any case behave adiabatically for fast enough time scale. The stability margin can be made larger increasing the heat sink (e.g. helium amount) and its efficiency in absorbing heat inputs (that is the heat transfer). This is typically the way followed in CICC for large, pulsed magnets which are designed for use in energy storage or thermonuclear fusion applications. The disturbance spectrum is dominated in these cases by electromagnetic energy coupling through ac losses, which are generally much larger than the enthalpy margin of the superconducting wire itself. Several options are possible to increase the helium amount and the heat transfer. In a force-flow conductor, for instance, the helium flows in channels inside the conductor, and the strands are subdivided to increase their wetted perimeter and improve turbulent heat transfer. Another option is to use superfluid helium, which has an exceedingly high heat transfer rate, in close contact with the wire. In any case the superconducting cable is in a *meta-stable* situation, namely it can be quenched by a large enough energy input. The art consists in reaching the desired stability margin for reliable operation with maximum operating current density.

The problem is in the fact that the calculation of the energy margin associated with a perturbation of arbitrary distribution in space and time waveform is a complex matter. All theories discussed so far have underlying approximations and limits, and the only manner to attack the general case is by numerical simulation of the non-linear heat balance. Even so the calculation remains a difficult task, involving accurate computation of heat conduction and possibly compressible helium flow in complex geometry, taking in account the non-linear material properties. In practice the numerical calculation of the stability margin is the virtual analog of an experiment, proceeding by trial and error to refine the approximation between the lower perturbation boundary, leading to the recovery, and the upper boundary, resulting in a quench. The techniques discussed in the previous sections, involving verification of the power balance and of the enthalpy margin, provide approximate calculations that are usually enough for scoping calculations and design, and to start the search for more intense numerical calculations. The following examples give the typical logic sequence followed to achieve stable operation of magnetic systems in all operating conditions.

Transient stability of the EU-LCT coil

The Euratom-Large Coil Task (EU-LCT) coil was built in the frame of the Large Coil Task project, a multinational effort to demonstrate the feasibility of a toroidal field system for a thermonuclear fusion reactor [45]. The coil was wound in a D-shape using the two-in-hand technique in seven double pancakes. The winding pack was epoxy impregnated under vacuum and enclosed in a thick steel casing which reacted most of the electromagnetic forces, see Fig. 44. At the nominal operating current of 11400 A the maximum field produced in the winding during full-array tests in the IFSMTF test facility was of 8.1 T, and the stored energy was about 100 MJ. The conductor itself, shown in Fig. 45, was obtained *Roebel*-cabling 23 rectangular NbTi strands (with copper stabiliser) around a central steel foil, and encasing this core in a steel jacket, producing a flat cable of 10 mm thickness and 40 mm width. The helium could flow between each strand within the leak-tight jacket. Each strand, 2.35 × 3.1 mm^2 in size, contained 774 NbTi filaments with a nominal diameter of 45 μm.

Figure 44. The EU-LCT coil in its casing.

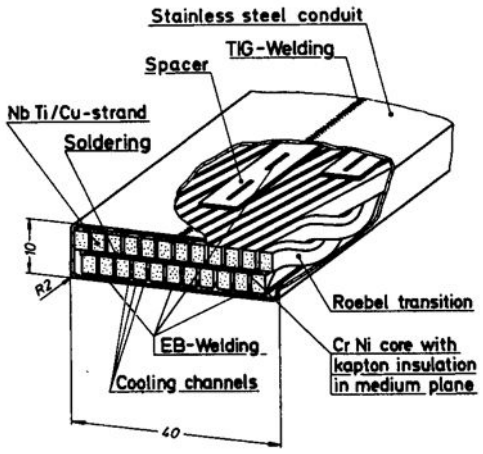

Figure 45. The EU-LCT cable.

The current density in the strands was around 70 A mm^{-2} in nominal conditions. This value is more than twice as high as the one of the BEBC conductor described earlier, and with an operating field increase from about 5 T in the BEBC magnet to about 8 T in the EU-LCT coil. The cooled perimeter of this complex configuration was estimated to be of the order of 165 mm, and at the nominal flow conditions the heat transfer coefficient was approximately 600 W m^{-2} K. If we calculate the Stekly coefficient for these specific conditions we obtain a value of $\alpha \approx 4$, much above the cryostable limit.

The disturbance spectrum during the operation of a TF coil in a fusion experiment is expected to be dominated by AC loss deposition during the field change associated with the sudden instability of the plasma column, or plasma *disruption*. Tests were performed on the EU-LCT coil pulsing an external coil and producing field changes up to 0.3 T with a time scale of 0.5 s. This deposited in the conductor an energy of the order of 15 mJ cm^{-3} of strand, without causing a quench [45]. Calculations and measurements showed that for heat inputs in a short time scale (0.5 ms) the stability margin was of the order of 10 to 30 mJ cm^{-3} of strand [46] in conditions comparable to the operating point of the cable. Over longer time scales the stability margin increased as more time was available to transfer heat to the helium.

No measurements are available for the conditions of the field pulse test quoted above, but a rough estimate, considering that the stability margin scales as the square-root of the time scale of the energy deposition [47], results in a minimum stability margin of the order of 100 mJ cm^{-3}, well above the energy deposited by ac loss. Indeed, the coil never had a spontaneous quench during testing.

The Tore Supra toroidal field magnet

Tore Supra [48] is a tokamak built in the 80's at the Centre d'Etudes de Cadarache (France). Its toroidal field (TF) magnet is completely superconducting, and operates in a stagnant superfluid helium bath. The TF magnet is composed of 18 circular coils, wound out of a monolithic composite conductor in 26 double pancakes. The double pancakes are separated by spacers that maintain electrical insulation but allow the free flow of helium around the conductor and insure a helium percentage in the winding pack of the order of 50 % of the conductor volume. The winding pack is kept under compression by an external steel casing which provides the tightness for the superfluid helium bath, which is maintained at approximately 1.8 K temperature and 1 bar pressure in normal operating conditions. At the operating current of 1400 A the maximum field produced on the winding pack is of 9 T, for a stored energy in the TF magnet of 610 MJ. The conductor (see Fig. 46) is a rectangular wire, of 2.8 × 5.6 mm^2 dimensions, with 11000 NbTi filaments of 23 μm diameter in a mixed copper and

CuNi matrix. The nominal NbTi cross section is 4.6 mm^2 and the copper cross section is 10 mm^2. At the operating conditions the current density in the wire is approximately 90 A mm^{-2}.

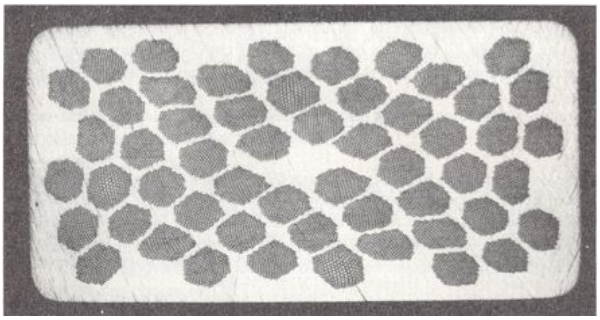

Figure 46. The Tore Supra strand.

For Tore Supra the tolerance against the disturbance spectrum was formulated requiring that the conductor must be able to recover:

- after a localised (length of the order of some mm) temperature excursion up to 30 K, or
- after a global (one full pancake) temperature excursion to 15 K, or
- after a plasma current disruption when the conductor is subjected to a field change of 0.6 T in 10 to 20 ms.

Stability in superfluid helium has peculiar characteristics as compared to the situation of a conductor wetted by boiling or supercritical normal helium. The main difference is the large heat transfer capability of superfluid helium [49]. At small heat fluxes the heat transport in superfluid helium is virtually infinite and the heat transfer coefficient h from the conductor to the helium is mostly governed by the Kapitza resistance at the wetted surface, with rather large values in the range of several thousands of W m^{-2} K. [49]. The picture is different for large heat fluxes. Both in steady state and transient conditions there is an upper limit to the heat flux that can be supported by superfluid helium before reaching the transition to the normal state, the so called *lambda* line. This limit depends both on the helium state and on the geometry. In the case of 1 bar subcooled superfluid helium, the operating condition of Tore Supra, a normal helium film forms at the wetted surface as soon as the peak heat flux is exceeded [50]. At the same time the heat transfer drops while the conductor temperature rises sharply.

The consequence is that for small heat fluxes, e.g. deriving from mechanical energy releases, the heat removal is such that the helium heat capacity available for stabilisation can be used completely. Larger energy depositions can be tolerated until the associated heat flux is below the maximum allowable value. This fact limits the available heat sink, as seen from the conductor side, to a fraction of the total helium volume. In the case of Tore Supra, calculations and experiments were performed to guarantee that the conditions given above could be satisfied. In particular a 60 m long cable had been tested in conditions comparable to the operation of the TF coil [51]. It was found that at the nominal operating current of 1400 A the cable was stable against a field pulse (1 T in 8 ms) comparable to the one required in the design specifications. The ac loss deposited by this field pulse was around 35 mJ cm^{-3} of wire, and in these conditions no normal zone could be detected. The average heat flux associated with such an ac loss is approximately 5 kW m^{-2}. This value, for the geometry of the cooling channel of the Tore Supra conductor, is well below the critical heat flux limit, which can be estimated in the order of 100 kW m^{-2} [49]. As the heat flux does not limit heat transfer, practically all the helium enthalpy from the operating temperature to the lambda transition is used for stabilisation. The typical helium enthalpy from 1.8 K to T_λ is of the order of 300 J m^{-3} of helium volume, that is approximately 150 J m^{-3} of strand volume. This last is a good estimate of the stability margin at normal operating conditions.

7 SUMMARY AND ADVANCED TOPICS

This chapter has presented the basic considerations and models that go into the achievement of stable superconductors. Overall, we can see the strategies presented above as a trade-off between the desired performance, and the allocated margin. One way to see this is to look at the schematic represetation in Fig. 47, where various stabilization strategies discussed are plotted in terms of the typical range of energy margin vs. the typical range of operating current density for which the strategy can be applied. The reader is warned that, as for the perturbation spectrum, this is only an order of magnitude represetation, and exceptions can deviate largely from the ranges identified there. Overall, however, we see that high operating current density is invariably associated with small energy margin. This implies that much effort must go in the control and reduction of the perturbation spectrum.

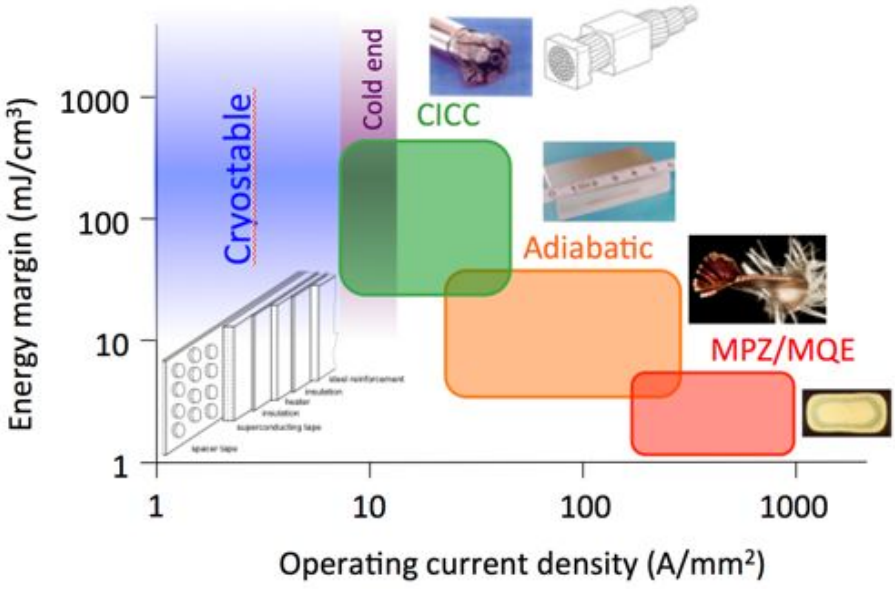

Figure 47. A scatter plot of typical range of energy margin vs. operating current density corresponding to the various stabilization strategies discussed in this chapter.

Enough is known on the mechanisms determining stability so that, in conjunction with other constraints, superconductors can be designed and optimized successfully. However, this does not mean the field is not open to new areas of research. As new magnet designs are proposed, and as more stringent requirements are imposed on the designer, areas of further study continue to open. In particular, work towards improving our understanding of stability under transient operating conditions, and the interaction of magnetic and thermal instabilities.

The details of transient local heat transfer are not fully known, nor understood, especially in complex flow geometries as often used for CICC's with cooling passages. As the heat transfer plays such an important role in the determination of the stable behaviour of a superconductor, this point is somewhat surprising, but must be understood in terms of the difficulties inherent to the precise measurement of flow and heat transport in a cryogenic fluid.

Stability depends in a synergistic manner on the DC and AC operating conditions of the cable in the coil. This is a main direction of research in the field of stability. In particular, in view of the applications to pulsed magnets, the interaction of stability, current distribution and AC losses in the cable is one of the main topics. The so called *ramp-rate* limit of operation for pulsed magnets (a decrease in the maximum achievable current at increasing field change rate) is an outstanding example

of this synergistic interaction. The appearance of such a phenomenon, explained so far in terms of non-uniform current distribution and a degradation of the stability margin of the cable, has alerted us to the difference between DC stability, with constant operating current and background field, and AC stability of the cable.

The distribution - and redistribution - of current among the strands and within the cable can have dramatic effects on stability. This statement applies to most cables used in technical applications (flat cables, CICC's, *super-stabilized* cables). Certainly the general solution of thermal, hydraulic and electromagnetic behaviour of a cable can be defined a formidable task. For this reason most of the efforts to understand current distribution in multistrand cables have been limited so far at the pure electromagnetic problem, neglecting the intrinsic coupling with the thermal behaviour [52, 53, 54]. Only recently more general attempts have been made at the coupled problem, and models have been presented for triplet of strands [55] and flat, accelerator cables [56].

During a thermal transient the current in a quenched strand tends to redistribute to the neighbouring strands driven by the voltage of the normal zone. The redistribution takes place across the transverse contact resistance (or at the joints in the case of insulated strands). The variation in the strand current induces a change in the Joule heating rate, coupling back to the temperature evolution. To model the redistribution process mutual inductive coupling of strands must be taken into account, while capacitive effects are negligible. Because a cable is strongly non-isotropic and because it has discrete contacts at the strand crossing, the first natural approach to a model of current distribution is the use of an electrical network modelling the strands as uniform current density sticks, coupled inductively and through localised cross resistances (see for instance Refs. [52] and [54]). This *network* approach is solved by Kirchoff's voltage and current laws, and requires that appropriate current *loops* are set for each degree of freedom in the cable cross section. It is very detailed, providing information on each strand cross-over contact, but it can result in a very large number of equations that are not conveniently coupled to a system of partial differential equations such as those given above.

An alternative, that has been used extensively for analytical studies, is to approximate the cross contacts as a continuous transverse conductance (see for instance [53]). A typical example is that of an ideal two-strand cable. In this case the governing equations become identical to that of an electrical transmission line with negligible capacitance, a well known problem in electromagnetics. This semi-continuum approach is also useful for stability studies.

Super-stabilized superconductors, used in large magnets with low intensity perturbation spectrum (detector magnets for high energy physics or SMES magnets), are a special field that is complex, but rather well understood. In superstabilized conductors a large amount of high conductivity material is added in parallel to the cable for protection. The distance of the stabilizer from the multifilamentary area, and its low resistivity, result in an increase of the current diffusion time out of the superconductor into the stabilizer. This effect is negligible within a strand, but becomes appreciable in the limit of large segregated stabilizers, when this time can become comparable or larger than the time scale of the evolution of the thermal transient. The cable is said to be *super-stabilized* if the time needed for current distribution is comparable or larger than the time-of-flight of the normal zone along the same section of conductor. In this type of cables the power dissipated by Joule heating during a transition to the normal state is initially much higher than the value reached after the current diffusion has taken place. After complete current diffusion the heating decreases to the asymptotic steady-state value corresponding to a uniform current distribution. The variation of Joule heating associated with the current diffusion affects the recovery of the cable. Furthermore the current diffusion can cause multiple stability boundaries, as well as stationary and travelling normal zones. Stability models for super-stabilized cables are obviously focussed on the effect of current distribution inside the massive stabilizer. Continuum models are commonly used to describe this process [57, 58]. The details of the superconducting cable, as well as heat transfer to the helium, are lesser issues.

Finally, the old trouble associated with flux jumps, at the beginning of the history of superconducting magnet technology, should not be forgotten. Indeed, the push for higher fields in compact magnets such as accelerator dipoles and quadrupoles, drives the need for current density to very high values in Nb_3Sn, in excess of 3000 A/mm^2 at 12 T and 4.2 K. At the same time, because of manufacturing reasons, the filaments of these high J_C materials are as large as 100 μm, and at present cannot be made much smaller than 30 μm. Such high J_C and large diameter causes flux jumps at low field (0 to 2 T), as should be expected. An unexpected additional problem is associated with a newly identified *self-field instability*, that can appear at intermediate and high fields (4 to 12 T) in strands of large critical current and diameter, of the oder of 1 mm or larger [59]. Such strands as required for large scale applications of high field magnets to help increasing the final size of the cable and ease protection. The drawback of a large strand diameter, associated with the very high values of J_C quoted earlier, is that the transport current tends to remain confined in a very thin skin of filaments, at the perifery of the multi-filamentary composite. A simple way to understand this instability is to consider this current distribution as generating a magnetic moment that can collapse and trigger an instability, much as a flux jump.

REFERENCES

[1] P.F. Chester, *Superconducting Magnets*, Rep. Prog. Phys., **XXX**, Part II, 561-614, 1967.

[2] M.A.R. LeBlanc, *Anomalous Transitions and New Phenomena in Hard Superconductors*, Phys. Rev., **124**, 1423, 1961.

[3] M.N. Wilson, *Superconducting Magnets*, Plenum Press, New York, 1983.

[4] Rutherford Laboratory Superconducting Applications Group, *Experimental and Theoretical Studies of Filamentary Superconducting Composites*, Journal of Physics, **D3**, 1517-1585, 1970.

[5] Y. Iwasa, *Conductor Motion in the Superconducting Magnet - A Review*, IIF-IIR-Commission A1/2 - Saclay, 125-136, 1981.

[6] H. Brechna, *Superconducting Magnet Systems*, Springer Verlag, 1973.

[7] D.N. Lyon, Int. J. Heat Mass Transfer, **7**, 1097, 1964.

[8] C. Johannes, Paper B 3, Cryogenic Engineering Conf., Boulder, 1970.

[9] C. Schmidt, Appl. Phys. Lett., **32** (12), 827, 1978.

[10] L.A. Yaskin, M.C. Jones, et al., *A Correlation for Heat Transfer to Supercritical Helium in Turbulent Flow in Small Channels*, Cryogenics, **17**, 549-552, 1977.

[11] P.J. Giarratano, V.D. Arp, R.V. Smith, *Forced Convection Heat Transfer to Supercritical Helium*, Cryogenics, **11**, 385-393, 1971.

[12] P.J. Giarratano, W.G. Steward, *Transient Forced Convection Heat Transfer to Helium During a Step in Heat Flux*, Trans. ASME, **105**, 350-357, 1983.

[13] W.B. Bloem, *Transient Heat Transfer to a Forced Flow of Supercritical Helium at 4.2 K*, Cryogenics, **26**, 300-308, 1986.

[14] G. Krafft, *Heat Transfer Below 10 K*, in *Cryogenic Engineering*, B.A. Hands ed., 171-192, Academic Press, 1986.

[15] A.R. Krantowitz, Z.J.J. Stekly, *A New Principle for the Construction of Stabilized Superconducting Coils*, Applied Physics Letters, **6**, 3, 56-57, 1965.

[16] Z.J.J. Stekly, J.L. Zar, *Stable Superconducting Coils*, IEEE Transactions on Nuclear Science, **12**, 367-372, 1965.

[17] E.U. Haebel, F. Wittgenstein, *Big European Bubble Chamber (BEBC) Magnet Progress Report*, Proceedings of 3rd International Conference on Magnet Technology, DESY, Hamburg, 874-895, 1970.

[18] B.J. Maddock, G.B. James, W.T. Norris, *Superconductive Composites: Heat Transfer and Steady State Stabilization*, Cryogenics, **9**, 261-273, 1969.

[19] M. Morpurgo, *The Design of the Superconducting Magnet for the "Omega" Project, Particle Accelerator*s, Vol I, Gordon and Breach Pub. Ltd, 1970.

[20] M.O. Hoenig, D.B. Montgomery, *Dense Supercritical Helium Cooled Superconductors for Large High Field Stabilized Magnets*, IEEE Trans. Mag., **11**, 2, 569, (1975)

[21] M.O. Hoenig, Y. Iwasa, D.B. Montgomery, *Supercritical-Helium Cooled "Bundle Conductors" and Their Application to Large Superconducting Magnets*, Proc. 5th Magn. Tech. Conf., Frascati, 519, (1975)

[22] M.O. Hoenig, Y. Iwasa, D.B. Montgomery, A. Bejan, *Supercritical Helium Cooled Cabled, Superconducting Hollow Conductors for Large High Field Magnets*, Proc. 6th Int. Cryo. Eng. Conf., Grenoble, 310, (1976)

[23] L. Dresner, *Stability-Optimized, Force-Cooled, Multifilamentary Superconductors*, IEEE Trans. Mag., **13**, 1, 670, (1977)

[24] L. Dresner, J.W. Lue, *Design of Forced-Cooled Conductors for Large Fusion Magnets*, Proc. 7th Symp. on Eng. Probs. of Fus. Res., Knoxville, Vol. I, 703, (1977)

[25] L. Dresner, *Stability of Internally Cooled Superconductors: a Review*, Cryogenics, **20**, 558, (1980)

[26] L. Dresner, *Superconductor Stability 1983: a Review*, Cryogenics, **24**, 283, (1984)

[27] M.O. Hoenig, D.B. Montgomery, *Cryostability Experiments of Force Cooled Superconductors*, Proc. 7th Symp. on Eng. Probs. of Fus. Res., Knowville, Vol. I, 780, (1977)

[28] M.O. Hoenig, D.B. Montgomery, S.J. Waldman, *Cryostability in Force Cooled Superconducting Cables*, IEEE Trans. Mag., **15**, 1, 792, (1979)

[29] M.O. Hoenig, *Internally Cooled Cabled Superconductors - Part I,* Cryogenics, **20**, 373-389, (1980)

[30] M.O. Hoenig, *Internally Cooled Cabled Superconductors - Part II,* Cryogenics, **20**, 427-434, (1980)

[31] J.R.Miller, J.W.Lue, S.S. Shen, J.C. Lottin, *Measurements of Stability of Cabled Superconductors Cooled by Flowing Supercritical Helium*, IEEE Trans. Mag., **15**, 1, 351, (1979)

[32] J.W. Lue, J.R. Miller, L. Dresner, *Stability of Cable-in-Conduit Superconductors*, J. Appl. Phys., **51**, 1, 772, (1980)

[33] J.W. Lue, J.R. Miller, *Parametric Study of the Stability Margin of Cable-in-Conduit Superconductors: Experiment*, IEEE Trans. Mag., **17**, 1, 757, (1981)

[34] L. Dresner, *Parametric Study of the Stability Margin of Cable-in-Conduit Superconductors: Theory*, IEEE Trans. Mag., **17**, 1, 753, (1981)

[35] L. Dresner, *Heating Induced Flows in Cable-in-Conduit Conductors*, Cryogenics, **19**, 653, (1979)

[36] J.R. Miller, J.W. Lue, S.S. Shen, L. Dresner, *Stability Measurements of a Large Nb3Sn Force-Cooled Conductor*, Adv. Cryo. Eng., **26**, 654, (1980)

[37] J.W. Lue, J.R. Miller, *Performance of an Internally Cooled Superconducting Solenoid*, Adv. Cryo. Eng., **27**, 227, (1982)

[38] J.V. Minervini, M.M. Steeves, M.O. Hoenig, *Experimental Determination of Stability Margin in a 27 Strand Bronze Matrix, Nb3Sn Cable-in-Conduit Conductor*, IEEE Trans. Mag., **21**, 2, 339, (1985)

[39] J.R. Miller, *Empirical Investigation of Factors Affecting the Stability of Cable-in-Conduit Superconductors*, Cryogenics, **25**, 552, (1985)

[40] T. Ando, M. Nishi, Y. Takahashi, K. Yoshida, S. Shimamoto, *Investigation of Stability in Cable-in-Conduit Conductors with Heat Pulse Duration of 0.1 to 1 ms*, Proc. 11th Int. Cryo. Eng. Conf., Berlin, 756, (1986)

[41] J.C. Lottin, J.R. Miller, *Stability of Internally Cooled Superconductors in the Temperature range 1.8 to 4.2 K*, IEEE Trans. Mag., **19**, 3, 439, (1983)

[42] J.H. Schultz, J.V. Minervini, *Sensitivity of Energy Margin and Cost Figures of Internally Cooled Cabled Superconductors (ICCS) to Parametric Variations in Conductor Design*, Proc. 9th Magn. Tech. Conf., Zurich , 643-646, (1985)

[43] A.P. Martinelli, Wipf, Proc. Appl. Sup. Conf. Annapolis, 1972.

[44] M.N. Wilson, Y. Iwasa, *Stability of Superconductors against Localized Disturbances of Limited Magnitude*, Cryogenics, 18, 17-25, 1978.

[45] D.S. Beard, W. Klose, S. Shimamoto, G. Vecsey, *The IEA Large Coil Task*, Fusion Engineering and Design, **7**, 1988.

[46] C. Schmidt, *Stability Tests on the Euratom LCT Conductor*, Cryogenics, **24**, 653-656, 1984.

[47] C. Schmidt, *Stability of Superconductors in Rapidly Changing Magnetic Fields*, Cryogenics, **30**, 501-510, 1990.

[48] A. Torossian, *TF-coil System and Experimental Results of Tore Supra*, Fusion Engineering and Design, **20**, 43-53, 1993.

[49] S.W. Van Sciver, *Helium Cryogenics*, Clarendon Press, Oxford, 1986

[50] P. Seyfert, J. Lafferranderie, G. Claudet, *Time Dependent Heat Transport in Subcooled Superfluid Helium*, Cryogenics, **22**, 401-408, 1982.

[51] R. Aymar, C. Deck, P. Genevey, F. Lefevre, C. Leloup, C. Meuris, S. Palanque, A. Sagniez, B. Turck, *Global Test of the Conductor for Tore Supra under Actual Working Conditions*, IEEE Transactions on Magnetics, **17**, 5, 2205-2208, 1981.

[52] A.A. Akhmetov, A. Devred, T. Ogitsu, Periodicity of Crossover Currents in a Rutherford-Type Cable Subjected to a Time-Dependent Magnetic Field , J. Appl. Phys., **75**, (6), 3176-3183, 1994.

[53] L. Krempaski, C. Schmidt, Theory of "Supercurrents" and their Influence on Field Quality and Stability of Superconducting Magnets, J. Appl. Phys., **78**, (9), 5800-5810, 1995.

[54] A.P. Verweij, H.H.J. ten Kate, Super Coupling Currents in Rutherford Type of Cables due to Longitudnal Non-homogeneities of dB/dt, IEEE Trans. Appl. Sup., **5**, (2), 404-407, 1995.

[55] N. Amemiya, O. Tsukamoto, Stability Analysis of Multi-Strand Superconducting Cables, IEEE Trans. Appl. Sup., **5** (2), 218-221, 1995.

[56] M.N.Wilson, R.Wolf, Calculation of Minimum Quench Energies in Rutherford Cables, IEEE Trans. Appl. Sup., **7** (2), 950-953, 1997.

[57] A. Devred, Investigation of Current Redistribution in Superstabilized Superconducting Winding when Switching to the Normal Resistive State, J. Appl. Phys., **65**, (10), 3963-3967, 1989.

[58] C.A. Luongo, R.J. Loyd, C.L. Chang, Current Diffusion Effects on the Performance of Large Monolithic Conductors, IEEE Trans. Mag., 25, (2), 1576-1581, 1989.

[59] B. Bordini B, L. Rossi, Self field instability in high Jc Nb3Sn strands with high copper residual resistivity ratio, IEEE Trans. Appl. Supercond., **19** (3), 2470-2476, 2009.